

1 *Author's Response*

2

3 We thank the Editor and the reviewer for their valuable comments. Most of the
4 comments suggested were followed. In the following, we extracted the comments
5 leading to major changes in the manuscript. *Major changes to the revised manuscript*
6 *are shown in blue.*

7

8 *Comments by the Editor:*

9 *1. P2 of the revised manuscript (Abstract), line 14–16:*

10 *Clarify sentence structure.*

11

12 **Original:**

13 P2 of the revised manuscript, line 14–16

14 The diurnal variations in the volume fraction of the volatile materials, HV, MV and LV
15 residuals were less than 15% for most of the particles except for the 40 nm ones,
16 although a daily maximum and a daily minimum were still observed.

17

18 **Revised:**

19 *In spite of the daily maximum and minimum, the diurnal variations in the volume*
20 *fractions of the volatile material, HV, MV and LV residuals were less than 15% for the*
21 *80–300 nm particles.*

22

23 **2. P3 of the revised manuscript (Section 1), line 28:**

24 *Add here a definition of volatile shrink factor (VSF) that is the ratio between the*
25 *particle size after exposed to elevated temperature to the original particle size. Then*
26 *it is easier to reformulate the end of the paragraph.*

27

28 **Original:**

29 P3 of the revised manuscript, line 28

30 Ambient aerosols have varying volatility properties based on their chemical
31 compositions. VTDMA was first introduced by Rader and McMurry (1986) to study
32 the behavior of aerosols upon thermal treatment.

33

34 **Revised:**

35 Ambient aerosols have varying volatility properties based on their chemical
36 compositions. VTDMA was first introduced by Rader and McMurry (1986) to study
37 the behavior of aerosols upon thermal treatment. *A volatility shrink factor (VSF) is*
38 *defined as the ratio of the particle size after exposed to elevated temperature to the*
39 *original size.*

40

41

42

43 **3. P4 of the revised manuscript (Section 1), line 8–11:**

44 *I think here you mean volatile shrink factors. Please reformulate.*

45

46 **Original:**

47 P4 of the revised manuscript, line 8–11

48 Particles with small volatile fractions are often assumed to be soot particles externally
49 mixed with particles with volatile materials at 300°C. Particles with larger volatile
50 fractions, which experienced size reductions of more than 10% upon heating at 300°C
51 in the VTDMA, were assumed to represent soot particles internally mixed (coated) with
52 the volatile materials (Philippin et al., 2004; Rose et al., 2011; Levy et al., 2014; Zhang
53 et al., 2016).

54

55 **Revised:**

56 Particles with small volatile fractions, *i.e. $VSF > 0.9$ at 300°C*, are often assumed to be
57 soot particles externally mixed with particles with volatile material at 300°C. Particles
58 with larger volatile fractions, *i.e. $VSF < 0.9$ at 300°C*, were assumed to represent soot
59 particles internally mixed (coated) with the volatile material (Cheng et al., 2006;
60 Wehner et al., 2009).

61 **4. P6 of the revised manuscript (Section 2.1.2), line 20–24:**

62 *The amount of external mixing can be seen with multiple modes in the distribution*
63 *after heating. Please clarify this section.*

64

65 **Response:**

66 A discussion of mixing state and its relationship with the modes in the size distribution
67 is added to line 29 onwards of P6. The sentences on line 20–27 of P6 were moved to
68 the end of the new discussion.

69

70 **Original:**

71 P6 of the revised manuscript, line 18 onwards

72 ... The *VSF* ranges for the LV, MV and HV particles upon heating at 300°C are defined
73 as follows: above 0.9, between 0.4 and 0.9 and below 0.4, respectively (Fig. 2) (Wehner
74 et al., 2004; Wehner et al., 2009). The LV particles are assumed to represent EC particles
75 externally mixed with the volatile materials, while MV and HV particles are assumed
76 to represent EC particles internally mixed with volatile materials. While the volatile
77 materials in the MV and HV particles are referred to as VM, those exist as external
78 mixtures with the LV, MV and HV particles are referred to as completely vaporized
79 (CV) particles. The CV particles evaporate completely without leaving behind any
80 residuals at 300°C. Excluding particle diffusional and thermophoretic losses, and
81 assuming that the residual material does not evaporate to the sizes below the detection
82 limit of the CPC (here 10 nm), the evaporation of VM and CV does not change the
83 number concentrations of LV, MV and HV particles.

84

85 The size distribution, $dN'/d\log D_p$ of the remaining particles (hereafter the residuals)
86 were measured by DMA₂ and CPC (Fig. 2b). Overall it took around one and a half to
87 two hours to complete a cycle of measurements which consisted of SMPS scans and V-
88 Mode measurements at 25°C, 100°C and 300°C. At each temperature, the sampling
89 time for six selected diameters from DMA₁ (40 nm, 80 nm, 110 nm, 150 nm, 200 nm
90 and 300 nm) took about half an hour and SMPS scans were made in-between. Hereafter,
91 notations with the superscript prime refer to the LV, MV or HV residuals measured by
92 DMA₂ and CPC after heating, while the corresponding ones without the prime refer to
93 the LV, MV or HV residuals in ambient aerosols prior to heating.

94

95 **Revised:**

96 ... The *VSF* ranges for the LV, MV and HV particles upon heating at 300°C are defined
97 as follows: above 0.9, between 0.4 and 0.9 and below 0.4, respectively (Fig. 2) (Wehner
98 et al., 2004; Wehner et al., 2009).

99

100 The size distribution, $dN'/d\log D_p$ of the remaining particles (hereafter the residuals)
101 were measured by DMA₂ and CPC (Fig. 2b). It can provide information of the mixing
102 state of the sampled aerosols. A uni-modal distribution indicates the presence of
103 internally-mixed particles exhibiting uniform size reduction upon heating, whereas a
104 multi-modal distribution indicates externally-mixed particles of different composition
105 and volatilities. In the multi-modal distribution, each mode represents particles of
106 similar composition and volatility. In this study, multiple modes of LV, MV and HV
107 were observed in the distribution after heating. The LV particles were assumed to
108 represent EC and non-volatile OC externally mixed with the volatile material, while
109 MV and HV particles were assumed to represent EC and non-volatile OC internally
110 mixed with volatile material. While the volatile material in the MV and HV particles
111 were referred to as VM, those exist as external mixtures with the LV, MV and HV
112 particles were referred to as completely vaporized (CV) particles. The CV particles
113 evaporated completely without leaving behind any residuals at 300°C. Excluding
114 particle diffusional and thermophoretic losses, and assuming that the residual material
115 did not evaporate to the sizes below the detection limit of the CPC (here 10 nm), the
116 evaporation of VM and CV did not change the number concentration of LV, MV and
117 HV particles.

118

119 Overall it took around one and a half to two hours to complete a cycle of measurements
120 which consisted of SMPS scans and V-Mode measurements at 25°C, 100°C and 300°C.
121 At each temperature, the sampling time for six selected diameters from DMA₁ (40 nm,
122 80 nm, 110 nm, 150 nm, 200 nm and 300 nm) took about half an hour and SMPS scans
123 were made in-between. Hereafter, notations with the superscript prime refer to the LV,
124 MV or HV residuals measured by DMA₂ and CPC after heating, while the
125 corresponding ones without the prime refer to the LV, MV or HV residuals in ambient
126 aerosols prior to heating.

127

128 **5. P10 of the revised manuscript (Section 3.1), line 21:**

129 *Size dependency on what?*

130

131 **Original:**

132 P10 of the revised manuscript, line 21

133 Furthermore, a size dependence was observed for 80 nm to 300 nm MV particles.

134

135 **Revised:**

136 Furthermore, [the number concentration of MV particles showed a size dependence in](#)
137 [the 80–300 nm particles.](#)

138

139

140

141 **6. P11 of the revised manuscript (Section 3.1), line 11:**

142 *Not standard terminology, please explain. Do you mean accumulation and coarse*
143 *mode?*

144

145 **Response:**

146 The droplet mode is a term used to describe the results of cloud processing (e.g. Seinfeld
147 and Pandis, 1998). It is in the fine mode of ambient particles. The sentence is removed
148 in the revised discussion (please refer to the next comment).

149

150 **Original:**

151 P11 of the revised manuscript, line 11

152 Yu et al. (2010) reported that the condensation and droplet modes of EC and OC in
153 urban sites of Guangzhou were approximately 400 nm and 900 nm, respectively.

154

155 **Revised:**

156 ~~Yu et al. (2010) reported that the condensation and droplet modes of EC and OC in~~
157 ~~urban sites of Guangzhou were approximately 400 nm and 900 nm, respectively.~~

158

159 7. *P11 of the revised manuscript (Section 3.1), line 12–13:*

160 *In terms of aerosol number, there is clear ultrafine mode in the fresh emissions, see*
161 *e.g. Rönkkö et al. (2014) or Karjalainen et al. (2014)*

162

163 *Rönkkö, T., Pirjola, L., Ntziachristos, L., Heikkilä, J., Karjalainen, J., Hillamo, R.*
164 *and Keskinen, J. (2014) Vehicle engines produce exhaust nanoparticles even when*
165 *not fuelled. Environmental Science & Technology, 2014, 48, 2043-2050.*

166

167 *Karjalainen, P., Pirjola, L., Heikkilä, J., Lähde, T., Tzamklozis, T., Ntziachristos, L.,*
168 *Keskinen, J. and Rönkkö, T. (2014). Atmos Environ.*

169

170 **Response:**

171 The discussion on the higher abundance of MV and LV in the larger size particles is
172 revised.

173

174 **Original:**

175 P11 of the revised manuscript, line 12–13

176 The higher abundance of MV and LV in larger size particles could also be explained by
177 the non-volatile primary particles. Yu et al. (2010) reported that the condensation and
178 droplet modes of EC and OC in urban sites of Guangzhou were approximately 400 nm
179 and 900 nm, respectively. The mode of fresh EC emitted from vehicles is also
180 approximately 400 nm (Huang et al., 2006). Larger particles also likely contain more
181 internally mixed aged aerosols (secondary pollutants) than the smaller ones.

182

183 **Revised:**

184 The higher abundance of MV and LV in the larger size particles could also be explained
185 by the aged particles arriving at the sampling site. Since the sampling site is located on
186 top of a mountain with an altitude of 150 m, the particles were likely aged upon arrival.
187 Non-volatile particles in the ultrafine modes from fresh emissions can be aged with
188 both non-volatile and volatile material, and became larger in size.

189

190 8. P15 of the revised manuscript (Section 3.3), line 23–24:

191 Please explain why.

192

193 **Response:**

194 The sentence will be removed since a minor revision of the *VSF* ranges would likely
195 lead to insignificant changes in the calculation of HV, MV and LV. We apologize for
196 the confusion.

197

198 **Revised:**

199 P15 of the revised manuscript, line 21–24

200 ~~Note that the fractions of HV, MV and LV have been traditionally defined based on the~~
201 ~~values of *VSF*, i.e. $HV < 0.4$; $0.4 < MV < 0.9$; $LV > 0.9$ (Wehner et al., 2009). The *VSF*~~
202 ~~distributions above suggest that these definitions using $VSF = 0.4$ and 0.9 may need to~~
203 ~~be re-visited in the future.—~~

204

205 **9. Section 3.4 New particle formation**

206 *This paragraph needs few references to NPF studies in China and globally as well.*

207

208 **Response:**

209 More discussions and references are added.

210

211 **Revised:**

212 Two new particle formation (NPF) events were observed in the campaign on 20 Feb
213 and 13 Mar 2014 (Fig. 3). Since VTDMA data were not available during the NPF event
214 on 13 Mar 2014, we only focus on the NPF event on 20 Feb 2014 which happened after
215 a cold front under a low PM_{2.5} concentration. On 20 Feb 2014, a sub-20 nm particle
216 mode was first observed at 12:00. This particle mode grew continuously until it reached
217 120 nm at 02:00 on 21 Feb 2014. In the VTDMA data, a sharp increase in the number
218 concentration of HV particles having an initial diameter of 40 nm was observed at 17:00
219 on 20 Feb 2014 (Fig. 10). This event is likely related to the growth of the newly formed
220 particles when they mixed with the volatile material accumulated via condensation or
221 adsorption. [The volatile material which extensively condensed on the pre-existing](#)
222 [particles could be sulfate, ammonium and organics. They were found to be the major](#)
223 [species contributing to particle growth in the NPF events at different locations \(Zhang](#)
224 [et al., 2004; Smith et al., 2008; Zhang et al., 2011; Yue et al., 2016\). Zhang et al. \(2004\)](#)
225 [observed that sulfate was always the first and the fastest species to increase in](#)
226 [concentration during an NPF event. They also suggested that photochemically formed](#)
227 [secondary organics contributed significantly to the growth of the ultrafine particles.](#)
228 [Recently, Yue et al. \(2016\) reported that sulfate, ammonium and organics were the main](#)
229 [contributors to particle growth in the NPF events in Taoyuan of the PRD region. As](#)
230 [these particles aged further, they grew larger as reflected in the increase in number](#)
231 [concentrations of larger MV particles and the increase in PM_{2.5} mass \(Fig. 10\). Similar](#)
232 [results were also observed in the study in Beijing by Wehner et al. \(2009\). Furthermore,](#)
233 [the growth of the newly formed particles can also be observed from the number size](#)
234 [distributions of the HV, MV and LV particles at different times on 20 and 21 Feb 2014](#)
235 [\(Fig. 11\). The mode of the HV particles increased from 40 nm at 17:00 to 80 nm at](#)
236 [21:00 on 20 Feb 2014. The mode stayed at 80 nm while the corresponding number](#)
237 [concentration decreased at 02:00 on 21 Feb 2014. In contrast, the number concentration](#)
238 [and diameter mode of the MV particles grew continuously. The HV and MV particle](#)
239 [concentrations and diameter modes underwent much smaller changes on the non-event](#)
240 [day of 28 Feb 2014 \(Fig. 11\).](#)

241

242

243 **10. P17 of the revised manuscript (Section 4), line 16:**

244 *Please provide references.*

245

246 **Original:**

247 P17 of the revised manuscript, line 16

248 The diurnal variations in the number and volume fractions of LV, MV and HV were
249 much less obvious in this study than in other studies likely because of the more stable
250 atmosphere and poorer dilution of aged aerosols in winter.

251

252 **Revised:**

253 The diurnal variations in the number and volume fractions of LV, MV and HV were
254 much less obvious in this study than in other studies (e.g. [Rose et al., 2011](#); [Cheng et
255 al., 2012](#); [Zhang et al., 2016](#)) likely because of the more stable atmosphere and poorer
256 dilution of aged aerosols in winter.

257

258

259

260 **11. P17 of the revised manuscript (Section 4), line 26–27:**

261 - *Please provide references.*

262 - *There is also previous works that point to this direction (non-volatile organics
263 as another possible component). E.g. [Häkkinen et al.](#)*

264

265 **Original:**

266 P17 of the revised manuscript, line 26–27

267 While previous studies have demonstrated soot as a major component of the non-
268 volatile residuals at 300°C measured by the VTDMA, this work identified non-volatile
269 organics as another possible component.

270

271 **Revised:**

272 While previous studies have indicated soot as a major component of the non-volatile
273 residuals at 300°C measured by the VTDMA (e.g. [Philippin et al., 2004](#); [Frey et al.,
274 2008](#)), [Häkkinen et al. \(2012\)](#) and this work identified non-volatile organics as another
275 possible component.

276

277

278

279 **12. References**

280 *Please be consistent with journal names etc.*

281

282 **Response:**

283 The reference list is updated such that the format is consistent now.

284

285

286

287 **References**

- 288 Cheng, Y. F., Eichler, H., Wiedensohler, A., Heintzenberg, J., Zhang, Y. H., Hu, M.,
289 Herrmann, H., Zeng, L. M., Liu, S., Gnauk, T., Brüggemann, E., and He, L. Y.:
290 Mixing state of elemental carbon and non-light-absorbing aerosol components
291 derived from in situ particle optical properties at Xinken in Pearl River Delta of
292 China, *J. Geophys. Res.-Atmos.*, 111, D20204, 2006.
- 293 Cheng, Y. F., Su, H., Rose, D., Gunthe, S. S., Berghof, M., Wehner, B., Achtert, P.,
294 Nowak, A., Takegawa, N., Kondo, Y., Shiraiwa, M., Gong, Y. G., Shao, M., Hu,
295 M., Zhu, T., Zhang, Y. H., Carmichael, G. R., Wiedensohler, A., Andreae, M.
296 O., and Pöschl, U.: Size-resolved measurement of the mixing state of soot in the
297 megacity Beijing, China: diurnal cycle, aging and parameterization, *Atmos.*
298 *Chem. Phys.*, 12, 4477-4491, 2012.
- 299 Frey, A., Rose, D., Wehner, B., Müller, T., Cheng, Y., Wiedensohler, A., and Virkkula,
300 A.: Application of the Volatility-TDMA Technique to Determine the Number
301 Size Distribution and Mass Concentration of Less Volatile Particles, *Aerosol Sci.*
302 *Technol.*, 42, 817-828, 2008.
- 303 Levy, M. E., Zhang, R., Zheng, J., Tan, H., Wang, Y., Molina, L. T., Takahama, S.,
304 Russell, L. M., and Li, G.: Measurements of submicron aerosols at the
305 California–Mexico border during the Cal–Mex 2010 field campaign, *Atmos.*
306 *Environ.*, 88, 308-319, 2014.
- 307 Philippin, S., Wiedensohler, A., and Stratmann, F.: Measurements of non-volatile
308 fractions of pollution aerosols with an eight-tube volatility tandem differential
309 mobility analyzer (VTDMA-8), *J. Aerosol Sci.*, 35, 185-203, 2004.
- 310 Rose, D., Gunthe, S. S., Su, H., Garland, R. M., Yang, H., Berghof, M., Cheng, Y. F.,
311 Wehner, B., Achtert, P., Nowak, A., Wiedensohler, A., Takegawa, N., Kondo, Y.,
312 Hu, M., Zhang, Y., Andreae, M. O., and Pöschl, U.: Cloud condensation nuclei
313 in polluted air and biomass burning smoke near the mega-city Guangzhou,
314 China – Part 2: Size-resolved aerosol chemical composition, diurnal cycles, and
315 externally mixed weakly CCN-active soot particles, *Atmos. Chem. Phys.*, 11,
316 2817-2836, 2011.
- 317 Seinfeld, J. H. and Pandis, S. N.: *Atmospheric chemistry and physics: from air pollution*
318 *to climate change*, 1998.
- 319 Smith, J. N., Dunn, M. J., VanReken, T. M., Iida, K., Stolzenburg, M. R., McMurry, P.
320 H., and Huey, L. G.: Chemical composition of atmospheric nanoparticles
321 formed from nucleation in Tecamac, Mexico: Evidence for an important role for
322 organic species in nanoparticle growth, *Geophys. Res. Lett.*, 35, L04808, 2008.
- 323

324 Wehner, B., Berghof, M., Cheng, Y. F., Achtert, P., Birmili, W., Nowak, A.,
325 Wiedensohler, A., Garland, R. M., Pöschl, U., Hu, M., and Zhu, T.: Mixing state
326 of nonvolatile aerosol particle fractions and comparison with light absorption in
327 the polluted Beijing region, *J. Geophys. Res.-Atmos.*, 114, D00G17, 2009.

328 Yu, H., Wu, C., Wu, D., and Yu, J. Z.: Size distributions of elemental carbon and its
329 contribution to light extinction in urban and rural locations in the pearl river
330 delta region, China, *Atmos. Chem. Phys.*, 10, 5107-5119, 2010.

331 Yue, D. L., Zhong, L. J., Zhang, T., J., S., L., Y., Q., Y. S., Y., Z., and Zeng, L. M.:
332 Particle Growth and Variation of Cloud Condensation Nucleus Activity on
333 Polluted Days with New Particle Formation: A Case Study for Regional Air
334 Pollution in the PRD Region, China, *Aerosol Air Qual. Res.*, 16, 323-335, 2016.

335 Zhang, Q., Stanier, C. O., Canagaratna, M. R., Jayne, J. T., Worsnop, D. R., Pandis, S.
336 N., and Jimenez, J. L.: Insights into the Chemistry of New Particle Formation
337 and Growth Events in Pittsburgh Based on Aerosol Mass Spectrometry, *Environ.*
338 *Sci. Technol.*, 38, 4797-4809, 2004.

339 Zhang, S. L., Ma, N., Kecorius, S., Wang, P. C., Hu, M., Wang, Z. B., Größ, J., Wu, Z.
340 J., and Wiedensohler, A.: Mixing state of atmospheric particles over the North
341 China Plain, *Atmos. Environ.*, 125, Part A, 152-164, 2016.

342 Zhang, Y. M., Zhang, X. Y., Sun, J. Y., Lin, W. L., Gong, S. L., Shen, X. J., and Yang,
343 S.: Characterization of new particle and secondary aerosol formation during
344 summertime in Beijing, China, *Tellus B*, 63, 382-394, 2011.

345

346 *Comments by Anonymous Referee #1:*

347

348 **1. Proper references need to be added to the intro part, especially for the comparison**
349 **with other VTDMA studies in paragraph 3.**

350

351 **Response:**

352 We apologize for not adding references properly in paragraph 3 of the Section 1. Please
353 find the revision below.

354

355 **Original:**

356 P4 of the revised manuscript (Introduction), line 5–13

357 ...Previous studies have demonstrated good agreement between the mass of black
358 carbon and the mass of particles with small volatile fractions, which experienced size
359 reductions of 5 to 10% upon heating at 300°C in the VTDMA. Various studies have
360 also used an VTDMA to estimate the mixing states of soot particles. Particles with small
361 volatile fractions are often assumed to be soot particles externally mixed with particles
362 with volatile materials at 300°C. Particles with larger volatile fractions, which
363 experienced size reductions of more than 10% upon heating at 300°C in the VTDMA,
364 were assumed to represent soot particles internally mixed (coated) with the volatile
365 materials (Philippin et al., 2004; Cheng et al., 2006; Frey et al., 2008; Wehner et al.,
366 2009; Rose et al., 2011; Levy et al., 2014; Zhang et al., 2016).

367

368 **Revised:**

369 ...Previous studies have demonstrated a good agreement between the mass
370 concentration of black carbon and the mass concentration of non-volatile particles that
371 experienced size reductions of 5 to 10% upon heating at 300°C in the VTDMA (Frey
372 et al., 2008). Various studies have also used the VTDMA to estimate the mixing states
373 of soot particles (e.g. Philippin et al., 2004; Rose et al., 2011; Levy et al., 2014; Zhang
374 et al., 2016). Particles with small volatile fractions, i.e. $VSF > 0.9$ at 300°C, are often
375 assumed to be soot particles externally mixed with particles with volatile materials at
376 300°C. Particles with larger volatile fractions, i.e. $VSF < 0.9$ at 300°C, were assumed
377 to represent soot particles internally mixed (coated) with the volatile materials (Cheng
378 et al., 2006; Wehner et al., 2009).

379

380

381 **2. Give clear definitions of all 5 air mass cluster in Table 3 in your manuscript.**

382

383 **Response:**

384 Definitions of the air masses were given at the beginning of Section 3.3 (Back trajectory
385 analyses).

386

387 **Original:**

388 P13 of the revised manuscript (Section 3.3), line 24–27

389 Clusters 1 and 3 are coastal and continental air masses, respectively, although both
390 originated from the northeast. Clusters 4, 5 and 6 represent continental air masses
391 originating from the northwest. Cluster 2 is a group of maritime air masses originating
392 from the East China Sea northeast or east of Guangzhou.

393

394

395 Table 3. Summary of concentrations of PM_{2.5}, OC, EC and the ratio of OC to EC
396 (OC/EC) in the five clusters.

	Cluster				
	Coastal	Maritime		Continental	
	1	2	3	4	5
Origin (to the site)	NE	NE/E	NE	NW	NW
PM _{2.5} (µg m ⁻³)	58.5 ± 24.4	58.9 ± 30.9	47.5 ± 28.4	33.9 ± 15.9	33.8 ± 19.3
OC (µg m ⁻³)	10.8 ± 6.01	10.84 ± 7.22	10.13 ± 6.89	5.51 ± 3.3	7.32 ± 2.75
EC (µg m ⁻³)	4.38 ± 2.97	4.98 ± 4.21	3.43 ± 3.12	1.8 ± 0.98	2.46 ± 0.59
OC/EC	2.83 ± 1.05	2.62 ± 1.03	3.65 ± 1.6	3.18 ± 1.26	2.94 ± 0.73

397

398

399 3. It is difficult to follow the scales of Fig. 5. All scales of these 12 subplot vary with
400 each other. Also for Fig. 6.

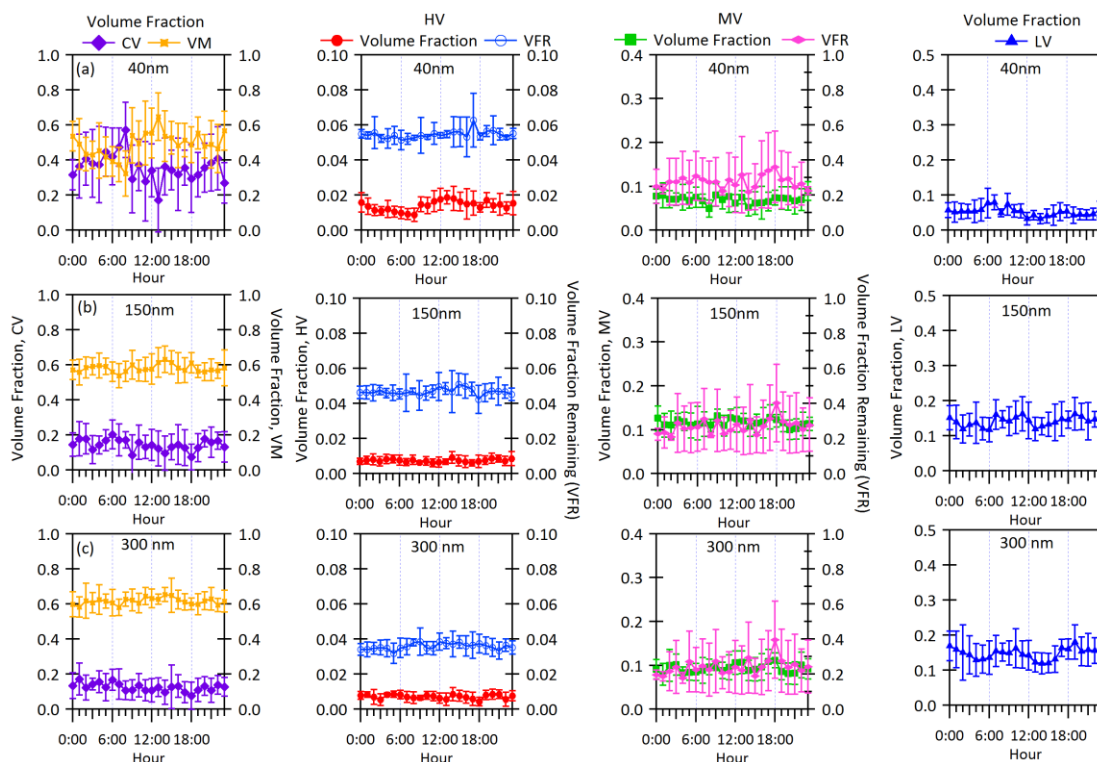
401

402 **Response:**

403 The scales of Fig. 5 and 6 are revised to be more consistent.

404

405 **Original:**



406

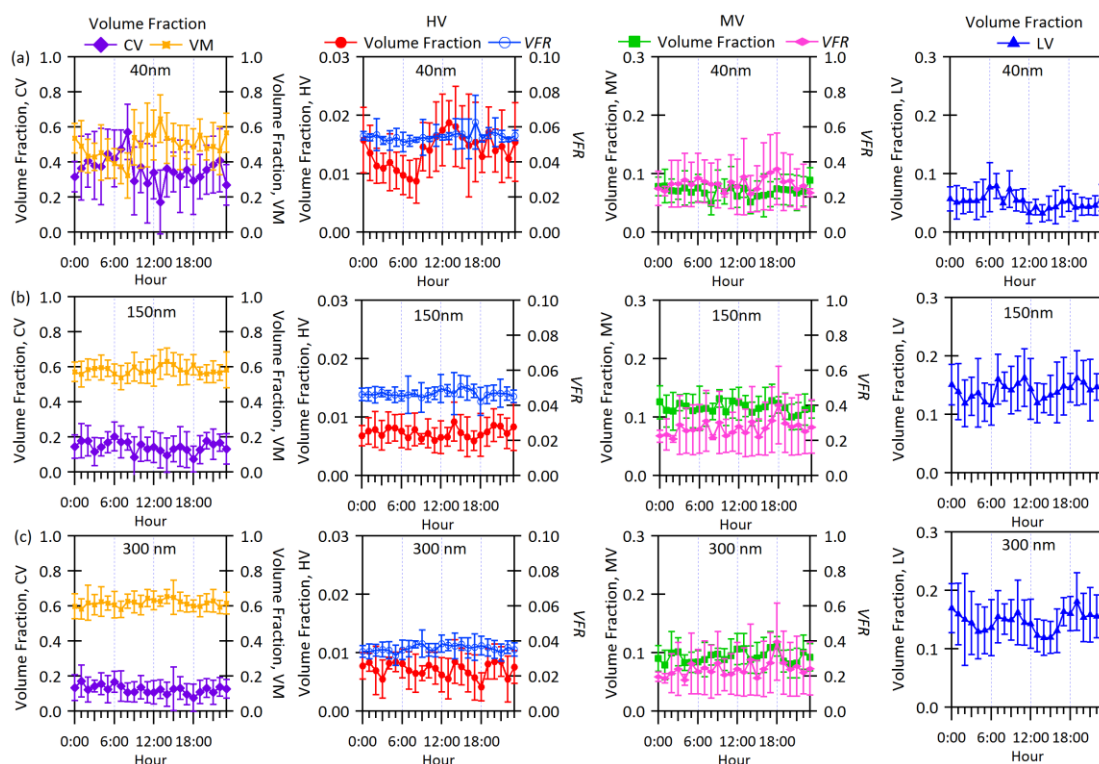
407 Fig. R1. Diurnal variations in volume fractions of (columns from left to right) CV, VM,
408 HV residuals, MV residuals and LV residuals in (a) 40 nm, (b) 150 nm and (c) 300 nm
409 particles. Diurnal variations in the volume fraction remaining (*VFR*) of HV and MV
410 particles are plotted on the right axis. Error bars represent one standard deviation.

411

412

413

414 **Revised:**



415

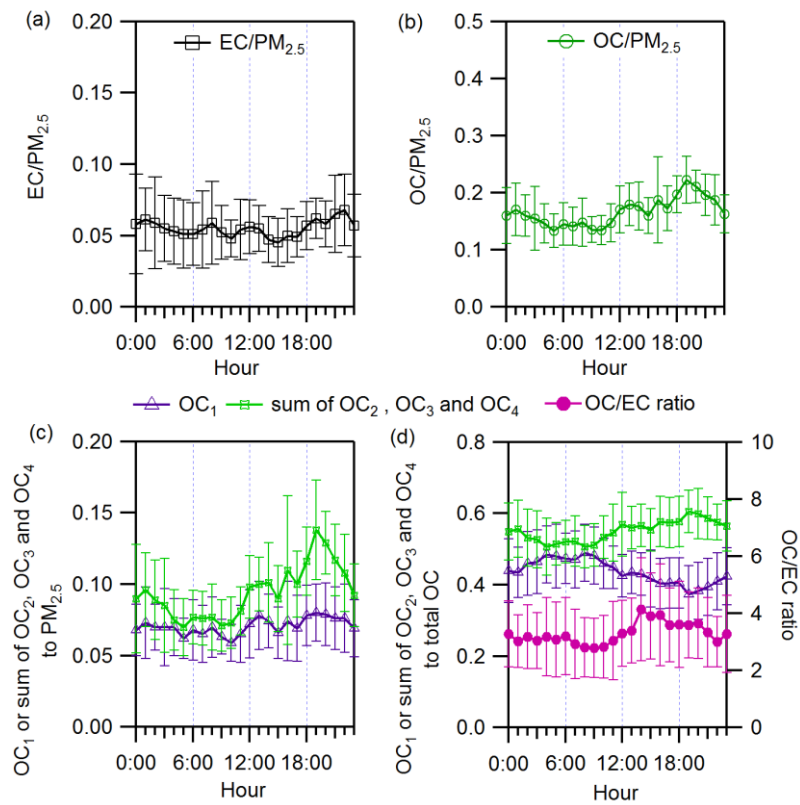
416 Fig. R2. Diurnal variations in volume fraction of (columns from left to right) CV, VM,
417 HV residuals, MV residuals and LV residuals in (a) 40 nm, (b) 150 nm and (c) 300 nm
418 particles. Diurnal variations in the volume fraction remaining (*VFR*) of HV and MV
419 particles are plotted on the right axis. Error bars represent one standard deviation.

420

421

422

423 **Original:**



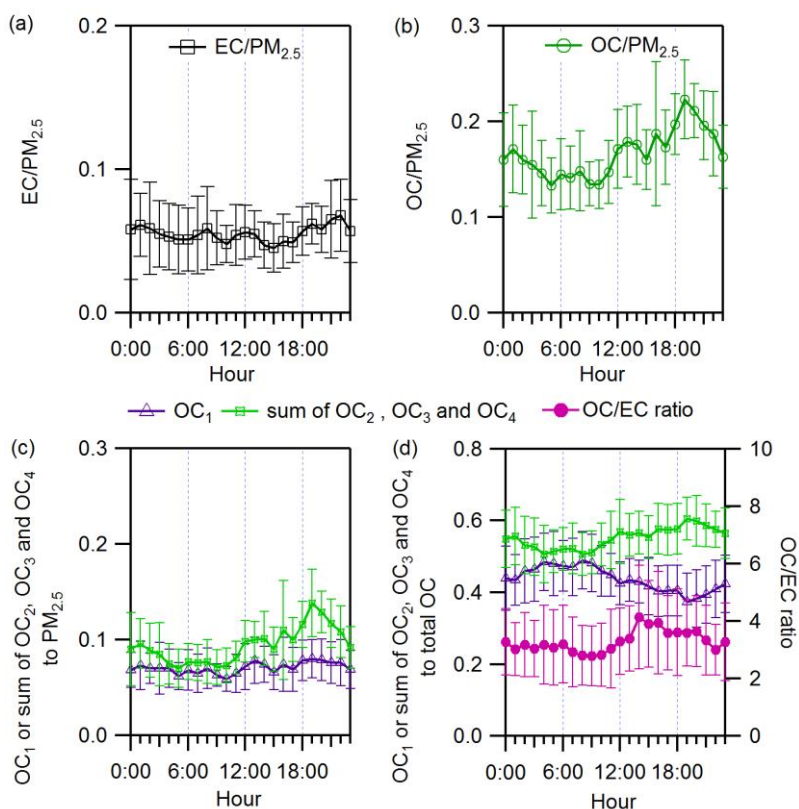
424

425 Fig. R3. Diurnal variations in the mass fractions of EC, OC, OC₁ and the sum of OC₂,
426 OC₃ and OC₄ in PM_{2.5}, the ratio of OC to EC, mass fractions of OC₁ and the sum of
427 OC₂, OC₃ and OC₄ to total OC in February and March. Error bars represent one standard
428 deviation.

429

430

431 **Revised:**



432

433 Fig. R4. Diurnal variations in the mass fractions of EC, OC, OC₁ and the sum of OC₂,
434 OC₃ and OC₄ in PM_{2.5}, the ratio of OC to EC, mass fractions of OC₁ and the sum of
435 OC₂, OC₃ and OC₄ to total OC in February and March 2014. Error bars represent one
436 standard deviation.

437

438 **4. In the conclusions, the author assumed the LV fraction to be EC, while in the**
439 **next paragraph the author concluded that non-volatile organics also contribute**
440 **to the non-volatile residuals. Please consider rewrite it to make it clear.**

441

442 **Original:**

443 P17 of the revised manuscript (Conclusions), line 11–14

444 This study presents the first VTDMA measurements in a suburban area of Guangzhou
445 in the Pearl River Delta, China during wintertime. The LV fraction was assumed to be
446 EC particles. These particles were externally mixed with volatile materials at 300°C
447 and contributed to less than 20% of the total particle number concentration at the
448 sampling site.

449

450 P18 of the revised manuscript (Conclusions), line 2–4

451 The mass closure analysis of EC and non-volatile OC and the total mass of the LV and
452 MV residuals also suggest that the non-volatile OC may have contributed to the non-
453 volatile residuals in our VTDMA measurements.

454

455 **Revised:**

456 P17 of the revised manuscript (Conclusions), line 11–14

457 This study presents the first VTDMA measurements in a suburban area of Guangzhou
458 in the Pearl River Delta region, China during wintertime. **The non-volatile material at**
459 **300°C in VTDMA measurements was assumed to be EC and non-volatile OC. The LV**
460 **particles, representing non-volatile material externally mixed with the volatile material,**
461 **contributed to less than 20% of the total particle number concentration at the sampling**
462 **site.**

463

464 P18 of the revised manuscript (Conclusions), line 2–4

465 **The mass closure analysis of EC and the total mass of LV and MV residuals also**
466 **indicated that EC alone cannot account for the mass of the non-volatile residuals. The**
467 **total mass of EC and the non-volatile OC gave a better closure with the total mass of**
468 **the LV and MV residuals, suggesting that the non-volatile OC may have contributed to**
469 **the non-volatile residuals in our VTDMA measurements.**

470

471 5. *Proof-reading is needed for the whole manuscript; there are quite many long*
472 *sentences along the whole text. Please consider rephrasing them.*

473

474 **Response:**

475 Some of the long sentences are rephrased or split into shorter sentences.

476 **Measurements of non-volatile aerosols with a VTDMA and**
477 **their correlations with carbonaceous aerosols in**
478 **Guangzhou, China**

479
480 **H. H. Y. Cheung¹, H. B. Tan², H. B. Xu³, F. Li², C. Wu¹, J. Z. Yu^{1,4} and C. K. Chan^{1,5,6}**

481 [1]{Division of Environment, Hong Kong University of Science and Technology, Hong Kong,
482 China }

483 [2]{Institute of Tropical and Marine Meteorology, China Meteorological Administration,
484 Guangzhou, China }

485 [3]{Sun Yat-sen University, Guangzhou, China }

486 [4]{Department of Chemistry, Hong Kong University of Science and Technology, Hong
487 Kong, China }

488 [5]{Department of Chemical and Biomolecular Engineering, Hong Kong University of
489 Science and Technology, Hong Kong, China }

490 [6]{School of Energy and Environment, City University of Hong Kong, Hong Kong, China }

491 Correspondence to: H. B. Tan (hbtan@grmc.gov.cn), C. K. Chan (chak.k.chan@cityu.edu.hk)

492

493 **Abstract**

494 Simultaneous measurements of aerosols ~~of varying volatilities~~ volatility and carbonaceous
495 matters were conducted at a suburban site in Guangzhou, China in February and March 2014
496 using a volatility tandem differential mobility analyzer (VTDMA) and an organic carbon/
497 elemental carbon (OC/EC) analyzer. Low volatility (LV) particles, with a volatility shrinkage
498 factor (*VSF*) at 300°C exceeding 0.9, contributed to 5% of number concentrations of the 40 nm
499 particles and 11–15% of the 80–300 nm particles. They were composed of non-volatile
500 materials ~~s~~ externally mixed with ~~the volatile ones~~ volatile material, and therefore did not
501 evaporate significantly at 300°C. Non-volatile materials ~~s~~ mixed internally with the volatile ~~ones~~
502 material were referred to as ~~the~~ medium volatility (MV, $0.4 < VSF < 0.9$) and high volatility
503 (HV, $VSF < 0.4$) particles. These ~~se~~ MV and HV particles contributed to 57–71% of number
504 concentrations ~~s~~ for the particles between 40 nm and 300 nm in size. The average EC and OC
505 concentrations measured by the OC/EC analyzer were $3.4 \pm 3.0 \mu\text{g m}^{-3}$ and $9.0 \pm 6.0 \mu\text{g m}^{-3}$,
506 respectively. Non-volatile OC evaporating at 475°C or above, together with EC, contributed to
507 67% of the total carbon mass. In spite of the daily maximum and minimum, the diurnal
508 variations in the volume fractions of the volatile materials, HV, MV and LV residuals were less
509 than 15% for ~~most of the~~ the 80–300 nm particles, ~~except for the 40 nm ones, although a daily~~
510 ~~maximum and a daily minimum were still observed~~. Back trajectory analysis also suggests that
511 over 90% of the air masses influencing the sampling site were well-aged as they were
512 transported at low altitudes (below 1500 m) for over 40 h before arrival. Further comparison
513 with the diurnal variations in the mass fractions of EC and the non-volatile OC in PM_{2.5} suggests
514 that the non-volatile residuals may be related to both EC and non-volatile OC in the afternoon,
515 during which the concentration of aged organics increased. A closure analysis of the total mass
516 of LV and MV residuals and the mass of EC or the sum of EC and non-volatile OC ~~was also~~
517 conducted. It suggests that non-volatile OC, in addition to EC, was one of the components of
518 the non-volatile residuals measured by the VTDMA in this study.

519

520 1 Introduction

521 Carbonaceous aerosols comprising organic carbon (OC) and elemental carbon (EC) or black
522 carbon (BC) are one of the major light absorption constituents and are abundant in particulate
523 matter (PM) (Rosen et al., 1978; Hansen et al., 1984; Japar et al., 1986; Chow et al., 1993;
524 Horvath, 1993; Lioussse et al., 1993; Fuller et al., 1999; Putaud et al., 2010; Tao et al., 2014;
525 Zhang et al., 2015). In China, the worsening of visibility degradation associated with PM is of
526 increasing concern in recent years. In particular, numerous studies on air pollution were carried
527 out in different cities in China including the Pearl River Delta (PRD) region which is a fast-
528 developing economic zone (Cheng et al., 2006; Wu et al., 2007; Andreae et al., 2008; Chan and
529 Yao, 2008; Gnauk et al., 2008; Tan et al., 2013a). In 2007, the mass concentrations of EC and
530 OC measured at an urban Guangzhou (GZ) site were reported to ~~be vary~~ from 6.8 to 9.4 $\mu\text{g m}^{-3}$
531 ³ and from 13.4 to 22.5 $\mu\text{g m}^{-3}$ respectively (Yu et al., 2010).

532 Soot particles are often characterized in terms of EC and BC, depending on whether they are
533 measured thermally or optically (Penner and Novakov, 1996; Lavanchy et al., 1999; Cheng et
534 al., 2011 and references therein). Their optical properties are distinct when they are freshly
535 produced (Novakov et al., 2003). After aging processes such as cloud processing, ~~reaction with~~
536 ~~other species~~ chemical reactions and coagulation, their structure, shape, size, mixing state and
537 thus optical properties change (Horvath, 1993; Lioussse et al., 1993; Ghazi and Olfert, 2012).
538 EC is typically measured by thermal method such as the OC/EC analyzer (Chow et al., 2007),
539 ~~whereas~~ BC ~~are is~~ optically measured using instruments such as aethalometer (Hansen et al.,
540 1984), multi-angle absorption photometer (Petzold and Schönlinner, 2004) and particle soot
541 absorption photometer (Virkkula et al., 2005). However, it is not possible to retrieve the
542 mixing state of soot particles ~~from above~~ with these techniques. To determine the mixing state
543 of soot particles, single particle soot photometer (Stephens et al., 2003), soot particle aerosol
544 mass spectrometer (Onasch et al., 2012) and Volatility Tandem Differential Mobility
545 Analyzer (VTDMA) (Philippin et al., 2004) have been used.

546 Ambient aerosols have varying volatility properties based on their chemical compositions.
547 VTDMA was first introduced by Rader and McMurry (1986) to study the behavior of aerosols
548 upon thermal treatment. A volatility shrink factor (VSF) is defined as the ratio of the particle
549 size after exposed to elevated temperature to the original particle size. Later Philippin et al.
550 (2004) ~~later~~ developed a VTDMA which ~~is was~~ capable of evaporating volatile materials in
551 aerosols at temperatures up to 300°C. Non-volatile ~~materials compounds~~ at 300°C, such as EC,
552 non-volatile organics and sea salt, can internally mix with (or be coated with) volatile materials.

553 Note that the terms “volatile” and “non-volatile” are here defined based on the operational
554 parameters and how the aerosol behave, when heated to at the heating temperature of 300°C in
555 the VTDMA. They are different from the volatilities defined under ambient conditions
556 (Donahue et al., 2009; Murphy et al., 2014) or in other measurement techniques (Twomey, 1968;
557 Pinnick et al., 1987; Huffman et al., 2009). The composition of these non-volatile residuals can
558 vary spatially and temporally ~~in VTDMA measurements~~. Previous studies have demonstrated a
559 good agreement between the mass concentration of black carbon BC and the mass concentration
560 of non-volatile particles with small volatile fractions, which that experienced size reductions of
561 5 to 10% upon heating at 300°C in the VTDMA (Frey et al., 2008). Various studies have also
562 used ~~an the~~ VTDMA to estimate the mixing states of soot particles. ~~Particles with small volatile~~
563 ~~fractions are often assumed to be soot particles externally mixed with particles with volatile~~
564 ~~materials at 300°C. Particles with larger volatile fractions, which experienced size reductions~~
565 ~~of more than 10% upon heating at 300°C in the VTDMA, were assumed to represent soot~~
566 ~~particles internally mixed (coated) with the volatile materials~~ (Philippin et al., 2004; Rose et al.,
567 2011; Levy et al., 2014; Zhang et al., 2016). Particles with small volatile fractions, i.e. $VSF >$
568 0.9 at 300°C, are often assumed to be soot particles externally mixed with particles with volatile
569 material at 300°C. Particles with larger volatile fractions, i.e. $-VSF < 0.9$ which experienced
570 size reductions of more than 10% upon heating at 300°C in the VTDMA, were assumed to
571 represent soot particles internally mixed (coated) with the volatile material (Cheng et al., 2006;
572 Wehner et al., 2009).

573 Organics also contribute to light absorption by atmospheric particles (Bond, 2001; Kirchstetter
574 et al., 2004; Chen and Bond, 2010). Laboratory studies have shown that organic aerosols may
575 form low volatility oligomers after aging for a long time (e.g. Kalberer et al., 2004). Huffman
576 et al. (2009) showed that highly oxygenated, aged organic aerosols exhibited similar or lower
577 volatility than the primary organic aerosols or the less oxygenated ~~ones particles~~. Recently,
578 Häkkinen et al. (2012) compared the residual mass derived from a volatility differential
579 mobility particle sizer (VDMPS) at 280°C with BC measured by an aethalometer and organics
580 measured by an Aerodyne aerosol mass spectrometer (AMS). It was found that the mass
581 fraction remaining (MFR) of non-BC residuals in VDMPS measurements, i.e. the difference
582 between the residual mass derived from a volatility differential mobility particle sizer at 280°C
583 and black carbon mass derived from an aethalometer, is was positively correlated with the mass
584 fraction of organics ~~measured by an in~~ AMS measurementsAMS.

585

586 In this study, simultaneous measurements of aerosols volatility and carbonaceous matter were
587 made at a suburban site in Guangzhou, China during wintertime in February and March 2014
588 using a VTDMA and a semi-continuous OC/EC analyzer, respectively. The volatility
589 measurements were made for ambient aerosols ranging from 40 nm to 300 nm in diameter. Here
590 residuals remaining after heating at 300°C in the VTDMA are referred to as non-volatile in this
591 study. We report the average values, time series and diurnal variations in the number and volume
592 fractions of the volatile and non-volatile materials, as well as the OC and EC concentrations.
593 We examine the relationships of the non-volatile materials upon heating at 300°C to EC and to
594 the non-volatile OC, based on analyses of the diurnal patterns and mass closures of the OC/EC
595 and VTDMA data. Finally, we discuss the influence of air mass origins on the volatility of the
596 sampled aerosols and concentrations of OC and EC based on back trajectory analysis.

597

598 **2 Methodology**

599 **2.1 Experimental**

600 **2.1.1 Measurement details**

601 The campaign ~~was taken~~took place at the China Meteorological Administration (CMA)
602 Atmospheric Watch Network (CAWNET) Station in Panyu, Guangzhou, China in summer from
603 July to September 2013 and in winter from ~~6~~February to ~~21~~March 2014~~,~~. The station~~which~~ is
604 operated by the Institute of Tropical and Marine Meteorology (ITMM) of the CMA. The Panyu
605 station is located at the center of the PRD region and on the top of Dazhengang Mountain (23°
606 00' N, 113°21' E) with an altitude of about 150 m (Fig. S1 in Supplemental Information) (Tan
607 et al., 2013a). It is about 120 m above the city ~~average elevation~~ and is surrounded by residential
608 neighborhoods with no significant industrial pollution sources nearby. Measurements of particle
609 number size distributions, volatility, mass concentrations of EC and OC in winter were made ~~in~~
610 ~~winter~~ from 6 February to 21 March 2014. Some of the measurements were not made
611 continuously due to maintenance work and hence only the periods with ~~both concurrent~~
612 VTDMA and OC/EC measurements were analyzed.

613 **2.1.2 VTDMA measurements**

614 We used a custom-made VTDMA based on a Hygroscopic TDMA system developed in ITMM
615 (Tan et al., 2013b), with the humidifier between the two DMAs replaced by a heated tube which

616 ~~effect induce~~ evaporation of volatile materials. In our VTDMA system shown in Fig. 1, ambient
617 aerosols ~~were~~ sampled by a PM_{2.5} inlet ~~first and subsequently~~ passed through a dryer at relative
618 humidity below 20%. The dry aerosols ~~then passed were then directed~~ through a neutralizer and
619 entered the first differential mobility analyzer (DMA₁) (Stream 1) to produce mono-disperse
620 aerosols of diameter between 40 nm and 300 nm, D_0 . The mono-disperse aerosols went either
621 ~~via~~ path (a) or (b) in Fig. 1 after leaving ~~the~~ DMA₁. In path (a), they (Stream 2) were directed
622 to a condensation particle counter (CPC, TSI Model 3772) to obtain particle counts, N_{D_0} . The
623 particle number size distribution of the ambient aerosols, $dN/d\log D_p$, was also measured by
624 varying the DMA₁ voltage (SMPS scan). Afterwards, the mono-disperse aerosols were directed
625 via path (b) to a heated tube for volatility measurement (V-Mode) sequentially at 25°C, 100°C
626 and 300°C. The heating tube was a 1/2", 80 cm long stainless steel tube with an inner diameter
627 of 8 mm. With a sample flow rate of 1 L min⁻¹, the resulting residence time in the heated section
628 of the VTDMA was 2.4 s. The estimated aerosol velocity on the center line was 0.33 m s⁻¹.
629 Compared to the residence time of 0.3 s to 1 s in other VTDMA systems (e.g. Brooks et al.,
630 2002; Philipin et al., 2004; Villani et al., 2007), the residence time in our VTDMA is assumed
631 to be long enough for the volatile materials to be effectively vaporized. After leaving the heating
632 tube, the flow entered a heat exchanger measuring 30 cm in length to ensure sufficient cooling
633 before entering DMA₂.

634 Upon heating ~~at 100°C and above~~, volatile components of particles such as sulfate, nitrate and
635 volatile organics ~~would~~ vaporize at different temperatures depending on their volatilities. ~~As~~
636 ~~mentioned in Section 1, the~~ volatility shrink factor, VSF , is defined as the ratio of particle
637 diameter after heating at temperature T , $D_{p,T}$, to ~~that the diameter~~ before heating, D_0 , ~~to indicate~~
638 ~~the size reduction of the ambient particles (Eq. (1)). The value of VSF is always smaller than or~~
639 ~~equal to one, depending on the amount of volatile materials vaporized at the heating temperature~~
640 ~~T .~~

$$641 \quad VSF(T) = \frac{D_{p,T}}{D_0} \quad (1)$$

642 ~~The VSF indicates the size reduction of the ambient particles upon heating. The value of VSF~~
643 ~~is always smaller than or equal to one, depending on the amount of volatile material vaporized~~
644 ~~at the heating temperature T .~~ The VSF is ~~also~~ used to divide the particles into three groups,
645 namely ~~the~~ low volatility (LV), medium volatility (MV) and high volatility (HV) particles. In
646 this study, we focus on the measurements made at 300°C. The VSF ranges for ~~the~~ LV, MV and
647 HV particles upon heating at 300°C are ~~defined as follows:~~ above 0.9, between 0.4 and 0.9 and
648 below 0.4, respectively (Fig. 2) (Wehner et al., 2004; Wehner et al., 2009). ~~The LV particles are~~

649 ~~assumed to represent EC particles externally mixed with the volatile materials, while MV and~~
650 ~~HV particles are assumed to represent EC particles internally mixed with volatile materials.~~
651 ~~While the volatile materials in the MV and HV particles are referred to as VM, those exist as~~
652 ~~external mixtures with the LV, MV and HV particles are referred to as completely vaporized~~
653 ~~(CV) particles. The CV particles evaporate completely without leaving behind any residuals at~~
654 ~~300°C. Excluding particle diffusional and thermophoretic losses, the evaporation of VM and~~
655 ~~CV does not change the number concentrations of LV, MV and HV particles.~~

656 The ~~new~~ size distribution, $dN'/d\log D_p$ of the remaining particles (hereafter the residuals) were
657 measured by DMA₂ and CPC ~~before they were heated at another temperature~~ (Fig. 2b). It can
658 provide information of the mixing state of the sampled aerosols. A uni-modal distribution
659 indicates the presence of internally-mixed particles exhibiting uniform size reduction upon
660 heating, whereas a multi-modal distribution indicates externally-mixed particles of different
661 composition and volatilities. In the multi-modal distribution, each mode represents particles of
662 similar composition and volatility. In this study, multiple modes of LV, MV and HV were
663 observed in the distribution after heating. The LV particles were assumed to represent EC and
664 non-volatile OC externally mixed with the volatile material, while MV and HV particles were
665 assumed to represent EC and non-volatile OC internally mixed with volatile material. While
666 the volatile material in the MV and HV particles were referred to as VM, those exist as external
667 mixtures with the LV, MV and HV particles were referred to as completely vaporized (CV)
668 particles. The CV particles evaporated completely without leaving behind any residuals at
669 300°C. Excluding particle diffusional and thermophoretic losses, and assuming that the residual
670 material did not evaporate to the sizes below the detection limit of the CPC (here 10 nm), the
671 evaporation of VM and CV did not change the number concentrations of LV, MV and HV
672 particles.

673 Overall it took around one and a half to two hours to complete a cycle of measurements which
674 consisted of SMPS scans and V-Mode measurements at 25°C, 100°C and 300°C. At each
675 temperature, the sampling time for six selected diameters from DMA₁ (40 nm, 80 nm, 110 nm,
676 150 nm, 200 nm and 300 nm) took about half an hour and SMPS scans were made in-between.
677 Hereafter, notations with the superscript prime refer to the LV, MV or HV residuals measured
678 by DMA₂ and CPC after heating, while the corresponding ones without the prime refer to the
679 LV, MV or HV residuals in ambient aerosols prior to heating.

680 2.1.3 OC/EC measurements

681 A semi-continuous Sunset OC/EC Analyzer (Model 4) was used to measure PM_{2.5} mass
682 concentrations of organic carbon and elemental carbon, m_{OC} and m_{EC} respectively, on an hourly
683 basis (Turpin et al., 1990; Birch and Cary, 1996; Wu et al., 2012). ~~With the~~ OC/EC Analyzer
684 ~~adopts~~ the ACE-Asia protocol (a NIOSH-derived protocol) ~~was adopted, wherein which~~ OC
685 ~~was evaporates~~ ~~evaporated~~ at four set temperatures of 310°C, 475°C, 615°C and 870°C with
686 pure helium (He) as ~~the a~~ carrier gas, ~~and whereas~~ EC ~~is was~~ combusted at temperatures
687 between 550°C and 870°C under He and 2% oxygen (O₂) (Schauer et al., 2003; Wu et al., 2012).
688 The OC contents ~~are were~~ named OC₁ to OC₄ based on the temperature protocol of the OC/EC
689 analyzer (Table 1). The mass of EC determined at different temperatures ~~will be as~~ grouped
690 together ~~for discussions in subsequent analysis~~.
691 ~~It is plausible that in~~ the VTDMA measurements, there were volatile or semi-volatile OC ~~which~~
692 ~~that~~ vaporize at 300°C or below. ~~These~~ ~~This~~ vaporized OC ~~are is~~ assumed to ~~be correspond to~~
693 OC₁, which ~~was vaporizes~~ ~~vaporized~~ at 310°C; although this OC/EC ~~set~~ temperature ~~is was~~
694 slightly higher than the ~~set~~ temperature of 300°C in the VTDMA. With this assumption, the
695 residuals ~~particles~~ of the VTDMA at 300°C (LV and MV residuals) are postulated to consist of
696 (1) OC₂ to OC₄, which ~~were~~ vaporized at 475°C and above, and (2) EC and other refractory PM
697 components. We have ignored the HV residuals as their contributions to the total volume of the
698 particles ~~are were~~ insignificant ~~when compared to in comparison with~~ LV and MV residuals
699 (Section 3.1). ~~In Section 3.5, we~~ will conduct a mass closure analysis based on the VTDMA
700 and OC/EC measurements to examine this assumption.

701 2.2 Data analysis

702 2.2.1 Number fractions

703 The number fractions of LV, MV and HV residuals ($\Phi'_{N,LV}$, $\Phi'_{N,MV}$ and $\Phi'_{N,HV}$, with their sum
704 being equal to unity) in Stream 2 on Fig. 1 were obtained from $dN'/d\log D_p$ measured by the
705 ~~CPCVTDMA~~. However, these fractions do not represent the actual number fractions of LV, MV
706 and HV particles ($\Phi_{N,LV}$, $\Phi_{N,MV}$ and $\Phi_{N,HV}$) before heating because ~~they have not taken into~~
707 ~~account the CV particles and particle diffusional and thermophoretic losses~~ ~~some of the particles~~
708 ~~can evaporate completely (CV) and due to diffusion and thermophoretic losses~~. The number
709 fraction of CV ($\Phi_{N,CV}$) ~~is was~~ first obtained by considering the number fractions ~~due to of~~ the
710 residuals ($1-\Phi_{N,CV}$) and the number concentrations at a selected diameter D_0 before heating (N_{D_0})

711 and after heating (N'):

$$712 \quad N_{D_0} \cdot \eta_{D_0} (1 - \Phi_{N,CV}) = N' \quad (2)$$

713 where η_{D_0} is the transport efficiency of particles.

714 ~~In Equation-Eq. (2) we assumes~~ that η is the same for LV, MV and HV particles. η accounts for
715 particle losses between DMA₁ and DMA₂ due to diffusion and thermophoretic forces (Philippin
716 et al., 2004), and it varies ~~with-as a function of~~ particle size and heating temperature. η at each
717 particle diameter and VTDMA temperature was determined ~~by-in~~ laboratory calibrations with
718 sodium chloride (NaCl) particles, which do not evaporate (i.e., $\Phi_{N,CV} = 0$) at the temperatures
719 used in our experiments. The transmission efficiency of NaCl of several selected diameters
720 ~~heated-atin~~ temperatures between 50°C and 300°C is provided in the supplemental information
721 (Fig. S2). From the known η and ~~field-measurements~~ observational data obtained with the
722 VTDMA providing N_{D_0} and N' , $\Phi_{N,CV}$ ~~was-obtained~~ can be calculated from Eq. (2). Afterwards,
723 $\Phi_{N,LV}$, $\Phi_{N,MV}$ and $\Phi_{N,HV}$ were obtained by renormalizing $\Phi'_{N,LV}$, $\Phi'_{N,MV}$ and $\Phi'_{N,HV}$ with $(1-\Phi_{N,CV})$
724 so that the sum of $\Phi_{N,LV}$, $\Phi_{N,MV}$, $\Phi_{N,HV}$ and $\Phi_{N,CV}$ equals ~~toed~~ unity.

725 2.2.2 Volume fractions

726 The volume fractions of LV, MV, HV residuals and CV ($\Phi_{V,LV}$, $\Phi_{V,MV}$, $\Phi_{V,HV}$ and $\Phi_{V,CV}$) at each
727 selected diameter D_0 are defined as the ratios of the volume of LV, MV, HV residuals and CV
728 to the total volume of the mono-disperse particles before heating. By assuming that the residuals
729 are ~~in~~ spherical in shape, $\Phi_{V,LV}$, $\Phi_{V,MV}$ and $\Phi_{V,HV}$ can be calculated by:

$$730 \quad \Phi_{V,i} = \frac{N_i \times \frac{\pi}{6} D_{p,i}^3}{N_{D_0} \times \frac{\pi}{6} D_0^3} = \Phi_{N,i} \cdot \frac{D_{p,i}^3}{D_0^3} \quad (3)$$

731 where N_i and $D_{p,i}$ are the number concentration and mean residual diameter of $i = LV, MV$ or
732 HV residuals.

733

734 For LV particles, it is assumed that D_0 and mean D_p are the same and hence $\Phi_{V,LV}$ is the same
735 as $\Phi_{N,LV}$. For MV and HV particles, the mean D_p is smaller than D_0 due to the evaporation of
736 volatile materials. The number weighted mean residual diameter (D_p) ~~is-was~~ is calculated by:

$$737 \quad D_{p,i} = \frac{\sum_j D_{p,i} \cdot N_{i,j}}{N_i} \quad (4)$$

738 where $D_{p,i}$ and $N_{i,j}$ are the residual diameter and number concentration of $i = MV$ or HV at the
739 75 diameter bins (j) of VSF, respectively.

740

741

The volume fractions of the evaporated materials ~~are-were~~ calculated from the volume fractions of the residuals. The calculation for $\Phi_{V,CV}$ ~~is-was~~ similar to that for $\Phi_{V,LV}$. Since the particle has completely vaporized, the vaporized volume is equivalent to the volume of the original particle. Hence, $\Phi_{V,CV}$ is the same as $\Phi_{N,CV}$:

$$\Phi_{V,CV} = \frac{N_{CV} \cdot \frac{\pi}{6} D_{p,CV}^3}{N_{D0} \cdot \frac{\pi}{6} D_0^3} = \Phi_{N,CV} \quad (5)$$

where $D_{p,CV} = D_0$. Since the sum of the total volume fraction of CV, VM and the residuals of LV, MV, HV ~~equals-equalled to~~ unity, $\Phi_{V,VM}$ was obtained after the above volume fractions were calculated. Furthermore, we also calculated the volume fraction remaining (*VFR*), defined as the volume ratio of the residual to its host particle, to aid our discussions later:

$$VFR_i = \frac{N_i \cdot \frac{\pi}{6} D_{p,i}^3}{N_i \cdot \frac{\pi}{6} D_0^3} = \frac{D_{p,i}^3}{D_0^3} \quad (6)$$

where N_i and $D_{p,i}$ are the number concentration and mean residual diameter of $i = MV$ or HV after heating, respectively.

2.2.3 Particle size distributions of number, volume and mass concentrations of LV, MV and HV residuals

Due to the differences in the size cuts of the VTDMA and the OC/EC analyzer, log-normal fits extrapolated to 5 μm were applied to the particle number size distributions of the residuals of LV, MV and HV ($dN/d\log D_{p,i}$, where $i = LV, MV$ or HV) to estimate the volume and then mass concentrations ~~(calculated later)~~ of the ambient aerosols for comparison with $\text{PM}_{2.5}$ OC/EC measurements. The volume size distributions ($dV/d\log D_{p,i}$) ~~are-were~~ calculated by:

$$\frac{dV}{d\log D_{p,i}} = \frac{dN}{d\log D_{p,i}} \cdot \frac{\pi}{6} D_{p,i}^3 \quad (7)$$

where $D_{p,i}$ is the mean residual diameter as defined in Section 2.2.2.

Volume (V) concentrations of LV, MV and HV residuals can then be calculated by integrating the area under the fitted curves. As we only focus on LV and MV, densities of 1.0 g cm^{-3} (Hitzenberger et al., 1999) and 1.5 g cm^{-3} are applied to V_{LV} and V_{MV} to obtain mass (m) concentrations of LV and MV residuals, respectively. The choice of the densities is based on the assumption that LV and MV residuals are dominated by soot and non-volatile OC, respectively.

771 3 Results and Discussions

772 3.1 Overview

773 The time series of meteorological conditions, particle number size distribution, PM_{2.5}, OC and
774 EC concentrations during the campaign are presented in Fig. 3. Overall, the campaign ~~came~~
775 was under the influence of the prevailing northerly wind with an average wind speed and
776 temperature (\pm one standard deviation) of $1.73 \pm 0.95 \text{ m s}^{-1}$ and $14.8 \pm 5.1^\circ\text{C}$, respectively. The
777 average PM_{2.5} concentration was $48 \pm 26 \mu\text{g m}^{-3}$. A few colder ~~front~~ periods were observed,
778 during which the wind speed increased and the temperature decreased. In general, the low wind
779 speed favored the accumulation of PM_{2.5}. During the campaign OC concentrations ranged from
780 0.5 to 47.0 $\mu\text{g m}^{-3}$ with an average of $9.0 \pm 6.0 \mu\text{g m}^{-3}$, while EC concentrations ranged from
781 0.2 to 23.0 $\mu\text{g m}^{-3}$ with an average of $3.4 \pm 3.0 \mu\text{g m}^{-3}$. OC₁, the most volatile group among OC₁
782 to OC₄ in OC/EC analysis, accounted for one-third of the total carbon mass (Fig. 4).

783 On ~~17 Feb-17, 12 and 17 Mar-12 and 17 2014~~, the daily-averaged PM_{2.5} concentrations exceeded
784 95 $\mu\text{g m}^{-3}$; and they were nearly twice the daily-averaged values ~~on of the~~ other days (Fig. 3,
785 shaded area in grey). Results of 72 h back trajectories (Stein et al., 2015; Rolph, 2016) showed
786 that air masses arriving at the site on or before these three days mostly originated from the
787 continental or oceanic area close to Eastern China (Fig. S3). The SMPS data also showed a
788 mode near 100 nm with a high particle number concentration (Fig. 3).

789 The temporal variation of the number concentration of MV particles having an initial diameter
790 of 80 nm or above tracked reasonably well with the accumulation of PM_{2.5} as the particles aged
791 and became more internally mixed (Fig. 3 and S4). Furthermore, the number concentration of
792 MV particles showed a size dependence in the 80-nm to 300 nm particles. There were days,
793 e.g., from 24 Feb to 10 Mar 2014, when the number concentration of 300 nm MV particles did
794 not track well with PM_{2.5} mass concentration. The mode of the total particle number size
795 distribution was below 100 nm and the number concentrations of 300 nm particles were low
796 (Fig. 3). PM_{2.5} mass concentration tracked better ~~with~~ the number concentrations of 80 nm to
797 150 nm MV particles (Fig. 4a to S4c) than those of 200 nm and 300 nm MV particles (Fig. S4d
798 and S4e).

799 The average number and volume fractions of CV, HV, MV and LV in VTDMA measurements
800 at 300°C are summarized in Table 2. VM is internally mixed with ~~(or coated on)~~ MV and HV
801 residuals, and hence does not have a separate contribution to number concentrations. Overall,
802 HV and MV particles, indicator for aged aerosols with internally mixed non-volatile and

803 volatile materials, accounted for 57% to 71% of the total particle number concentration. Non-
804 volatile materials (LV, MV and HV residuals) accounted for 15% to 26% of the total volume of
805 selected particles before heating. While the CV and HV fractions were larger in the finest
806 particles selected ($D_0 = 40$ nm), MV and LV were more abundant in larger particles ($D_0 > 80$
807 nm). As in Rose et al. (2006), fresh emissions like soot adsorbed or absorbed volatile materials
808 during atmospheric processing. The smaller particles grew to a greater extent faster than the
809 larger ones because of their higher ratios of surface area to volume. When they were heated in
810 the VTDMA at 300°C, these smaller particles reduced more substantially in size, as reflected
811 in the higher CV and HV fractions and lower MV and LV fractions. The higher abundance of
812 MV and LV in the larger size particles could also be explained by the the aged non-volatile
813 primary particles arriving at the sampling site. Since the sampling site is located on top of a
814 mountain with an altitude of 150 m, the particles were likely aged upon arrival. Non-volatile
815 particles in the ultrafine modes from fresh emissions can be aged with both non-volatile and
816 volatile material, and became larger in size. Yu et al. (2010) reported that the condensation and
817 droplet modes of EC and OC in urban sites of Guangzhou were approximately 400 nm and 900
818 nm, respectively. The mode of fresh EC emitted from vehicles is also approximately 400 nm
819 (Huang et al., 2006). The larger particles also likely contain more internally mixed aged aerosols
820 (secondary pollutants) than the smaller ones. The larger particles can contain more internally
821 mixed aged aerosol mass (secondary pollutants) than the smaller ones. Nevertheless, the
822 detection limit of the downstream DMA and CPC in the VTDMA system is 10 nm. ~~It was~~
823 ~~assumed that the residuals having a diameter below 10 nm were small enough to be considered~~
824 ~~as completely vaporized. However, such assumption would lead to~~ The particles with diameters
825 below the detection limit leads to an overestimation of CV and an underestimation of the non-
826 volatile residuals for the finest particles selected (with an initial diameter of 40 nm).

827 3.2 Diurnal variations

828 Figure 5 shows ~~the~~ diurnal variation in the fraction of CV, HV residual, MV residual, LV
829 residual and VM in the total volume of particles of dry initial diameters of 40, 150 and 300 nm.
830 For 40 nm particles, a clear maximum and minimum of the fraction of CV, VM and HV
831 residuals are observed at 08:00 and 13:00, respectively. The diurnal variation of the HV and
832 MV particles in the 40 nm particles was clearer in terms of number fraction (Fig. S5).
833 Furthermore, the trend of CV ~~is was~~ opposite to those of VM, HV and MV. The increase of CV
834 in the 40 nm particles and to a lesser extent of LV in the 150 nm and 300 nm particles in the

835 morning is consistent with traffic pattern, ~~where freshly~~ Fresh emissions of emitted volatile
836 and non-volatile materials, likely OC and EC, ~~are were~~ externally mixed and contributed to CV
837 and LV, respectively. As time progresses in a day, the highly volatile species (CV) which were
838 freshly emitted in the morning, may evaporate and react to form less volatile particles and
839 become VM instead of CV Robinson et al. (2007). Alternatively, these CV particles could also
840 coagulate with smaller particles to form VM containing particles. Less fresh emissions with
841 more CV particles turning into VM on MV and HV particles ~~can could~~ explain the trend that
842 the number and volume fractions of CV decreased while those of MV and HV increased (Fig.
843 5 and Fig. S5).

844 We also used the diurnal variations in the volume fraction remaining (*VFR*), again defined as
845 the volume ratio of the residual to its *host* particle (not to the total volume of all particles), to
846 examine the size changes of the non-volatile residuals of HV and MV particles. The *VFR* of
847 HV did not exhibit any obvious diurnal variations but the *VFR* of MV peaked near 18:00. The
848 *VFR* of the 40 nm MV particles increased after 14:00 while those of the 150 nm and 300 nm
849 MV particles increased after 15:00. Since the *VFR* of HV and MV were relatively constant
850 during the day, the increase in the VM fraction after the morning rush hours ~~is likely~~ could be
851 attributed to the increase in the number concentrations of the HV and MV particles instead of
852 changes in the amount of VM on the MV or HV residuals.

853 The diurnal variations for particles larger than 80 nm were much less obvious than those for 40
854 nm particles in this study and in others (Rose et al., 2011; Cheng et al., 2012; Zhang et al.,
855 2016). In winter, the atmosphere is more stable, resulting in a poorer dilution of aged particles
856 with the less polluted aerosols from higher up (Rose et al., 2006). When the aged pollutants
857 were trapped near the ground ~~surface~~, the effect of aging of fresh emissions weakened.
858 Therefore, although a daily maximum and a daily minimum were still observed for particles
859 larger than 80 nm, the variation was mostly within 15%.

860 The diurnal variations in the mass fractions of OC and EC in PM_{2.5} provided further insights to
861 the observations above (Fig. 6). The OC and EC data on Mar 12 and 17 were excluded since
862 they were more than two standard deviations higher than those on other days. Subtle morning
863 peaks between 06:00 and 10:00 were observed for the volume fraction of LV residuals (Fig. 5).
864 A similar peak was observed for the mass fraction of EC in PM_{2.5} in the morning (Fig. 6). This
865 suggests that the LV particles may be related to the EC from vehicle emissions in the morning.
866 This EC was relatively less aged and externally mixed with the other volatile materials. In the
867 late afternoon, the LV residuals showed another peak between 17:00 and 19:00 whereas the

868 mass fraction of EC in PM_{2.5} exhibited a minimum at 15:00, after which it increased
869 continuously. The continuous increase in EC at night is likely related to the increase of heavy-
870 duty diesel ~~vehicles traffic~~ (Zhang et al., 2015), which was restricted during daytime (Bradsher,
871 2007).

872 Although OC₁ contributed to about half of the total OC mass, the diurnal variation in the mass
873 fraction of OC in PM_{2.5} was driven by the total mass of OC₂, OC₃ and OC₄ (OC₂₋₄), which
874 reached a minimum between 05:00 and 09:00 and increased until 19:00. OC can be attributed
875 to both primary and secondary sources. The increased mass fraction of OC in PM_{2.5} and OC-
876 to-EC ratio in the afternoon suggest that the sources of OC were less related to traffic but more
877 to the aging and formation of secondary organic aerosols (Turpin et al., 1990; Chow et al., 1996).
878 These OC₂, OC₃ and OC₄ may be highly oxygenated species or oligomers that are less volatile
879 than primary or less oxygenated organics (Kalberer et al., 2004; Huffman et al., 2009).

880 It is interesting to note that the volume fraction of the LV residuals and the *VFR* of MV particles
881 at different sizes showed a dip in the afternoon (Fig. 5, third column from the left). The *VFR* of
882 40 nm MV particles showed a dip at 14:00 while those in 150 nm and 300 nm particles showed
883 a dip at 15:00. The volume fraction of LV residuals in 150 nm and 300 nm particles reached a
884 minimum at 13:00 and 15:00, respectively. Because EC decreased between 12:00 and 15:00,
885 the increase in the volume fraction of LV residuals in 150 nm particles since 13:00 and the *VFR*
886 of 40 nm MV particles since 14:00 may be related to the increased presence of aged organics
887 as well as the EC particles which aged via coagulation and condensation.

888 3.3 Back trajectory analyses

889 We calculated ~~the~~ 72 h back trajectories of ~~the~~ air masses arriving at the sampling site (23°00
890 N, 113°25' E) at 4 h intervals (at 00:00, 04:00, 08:00, 12:00, 16:00 and 20:00 local time, UTC
891 +8) using the PC version of the HYSPLIT4 (Hybrid Single Particle Lagrangian Integrated
892 Trajectory, version 4) model (Stein et al., 2015; Rolph, 2016). Archived meteorological data
893 from the Global Data Assimilation System (GDAS) 1-deg was employed and the receptor
894 height was set at 500 m above ground level (a.g.l.). The 191 back trajectories calculated were
895 grouped into six clusters based on their spatial distribution (Fig. 7).

896 Overall, the sampling site was mostly affected by northwesterly and northeasterly air masses.
897 Clusters 1 and 3 are coastal and continental air masses, respectively, although both originated
898 from the northeast. Clusters 4, 5 and 6 represent continental air masses originating from the
899 northwest. Cluster 2 is a group of maritime air masses originating from the East China Sea

900 northeast or east of Guangzhou. While the air masses in cluster 6 were transported at relatively
901 high speeds and altitudes (over 3000 m a.g.l.), the air masses in all the other clusters were
902 transported at an altitude below 1500 m a.g.l. for over 40 h before arriving at the site.
903 ~~Nevertheless, As the~~ air masses in cluster 6 only ~~persisted-occurred~~ for less than three days- and
904 since the corresponding VTDMA and OC/EC data were sometimes unavailable, cluster 6 will
905 be excluded from the following discussion.

906 The average PM_{2.5}, OC and EC concentrations associated with the air masses from the northeast
907 of Guangzhou (clusters 1, 2 and 3) were higher than those from the northwest (clusters 4 and 5,
908 Table 3). Days associated with the coastal and maritime air masses were more polluted than
909 days associated with continental air masses for several reasons. First, south China as a region
910 is often affected by the high pressure system moving eastward or southward from the continent
911 out to sea in winter. When the maritime or coastal air streams entered from the southeast of the
912 sampling site at Panyu, the atmosphere at the sampling site became more stable with low local
913 wind speeds (e.g. the polluted days on Feb 17 and Mar 12, 16 and 17, Fig. 3 and S3). The local
914 pollutants accumulated and the city was also affected by pollutants from the southeastern areas
915 of the site (e.g. Shenzhen, Nansha and Dongguan). Second, land-sea breeze ~~eyeles-circulation~~
916 were observed when the sampling site was under the influence of maritime air masses from Mar
917 18 to 20. During the day, southeasterly wind prevailed and the wind speed was higher. In the
918 evening, the southeasterly wind was gradually replaced by a southwesterly or northwesterly
919 wind and the wind speed decreased (Fig. 3). The cycle started again in the morning when the
920 westerly wind was gradually replaced by southeasterly wind. Such land-sea breeze effects can
921 result in an effective redistribution and accumulation of air pollutants within the PRD region
922 (Lo et al., 2006).

923 Furthermore, PM_{2.5} in the northeastern parts of China can exceed 200 $\mu\text{g m}^{-3}$ due to both
924 enhanced emissions from coal combustion for heating and poor dispersion during wintertime
925 (Gu et al., 2014). Under the influence of the prevailing northerly or northeasterly wind in China,
926 these pollutants were often transported to southern China and the East China Sea (Chen et al.,
927 2012). The pollutants might also have accumulated when the maritime air masses spent about
928 two days across Taiwan and the coast of south China. In contrast, continental air masses in
929 cluster 5 moved slightly faster, and were often associated with the cold front period during
930 which the local wind speed and pressure increased but the temperature decreased (Fig. 3). As
931 the cold air masses passed through the city, dispersion and clearance of pollutants were
932 promoted, resulting in lower PM_{2.5} concentrations (Tan et al., 2013a). Therefore, unlike in other

933 coastal cities like Hong Kong (Lee et al., 2013), in Panyu the maritime air masses could lead to
934 more severe pollution than the continental ones in winter.

935 The five clusters were further analyzed to study the influence of air mass history on aerosol
936 volatility. The number fractions of CV, HV, MV and LV of the six selected diameters in
937 VTDMA measurements are regrouped based on the clusters as shown in Fig. 8. The total
938 number fractions of the non-volatile residuals (sum of HV, MV and LV) were similar in all
939 clusters. The maritime air masses (cluster 2) had a slightly higher fraction of LV particles while
940 the continental air masses originating from the northwest of the site (clusters 4 and 5) had a
941 higher fraction of HV particles. Although the air masses in clusters 1 and 5 originated from
942 farther-further away and traveled at relatively higher speeds than those in clusters 2, 3 and 4,
943 all the clusters involved transport at low altitudes (below 1500 m) for over 40 h, likely due to
944 the generally lower mixing heights in winter. Therefore, it is plausible that the aerosols particles
945 in these air masses were all well-aged upon arrival. Similar results were observed in Beijing
946 by Wehner et al. (2009). This could be another reason for the lack of size dependence of the
947 number, volume fractions and diurnal variation for the particles larger than 80 nm. When the
948 transported air masses mixed with the local pollutants, the size dependence of the number
949 fractions of different volatility groups as well as the aging of local emissions was further
950 reduced.

951 We also examined the volatility shrink factor (*VSF*) distributions of 40 nm, 110 nm and 300 nm
952 particles upon heating at 300°C (Fig. 9). Log-normal fittings with a three-peak solution were
953 applied to the distributions. The average *VSF* modes of the peaks were located at 0.38 ± 0.021
954 (peak 1), 0.60 ± 0.066 (peak 2) and 0.95 ± 0.007 (peak 3), respectively. The standard deviation
955 of the corresponding normal distribution (σ) of peak 3 was the smallest among the three peaks
956 ($\sigma < 0.1$). For the same particle size, the *VSF* distributions in the *VSF* range between 0.3 and
957 0.8 in cluster 5 was relatively more uni-modal than those of other clusters (Fig. 9b and 9c). This
958 suggests that the composition in cluster 5 was more homogeneous. Cluster 1 also consisted of
959 long-range transported air masses but they likely passed through areas that are more polluted
960 and mixed with different types of pollutants. ~~Note that the fractions of HV, MV and LV have~~
961 ~~been traditionally defined based on the values of *VSF*, i.e. $HV < 0.4$; $0.4 < MV < 0.9$; $LV > 0.9$~~
962 ~~(Wehner et al., 2009). The *VSF* distributions above suggest that these definitions using $VSF =$~~
963 ~~0.4 and 0.9 may need to be re-visited in the future.~~

964 3.4 New particle formation

965 Two new particle formation (NPF) events were observed in the campaign on 20 Feb and 13
966 Mar [2014](#) (Fig. 3). Since VTDMA data were not available during the NPF event on 13 Mar
967 [2014](#), we only focus on the NPF event on 20 Feb [2014](#) which happened after a cold front under
968 a low PM_{2.5} concentration. On 20 Feb [2014](#), a sub-20 nm particle mode was first observed at
969 12:00. This particle mode grew continuously until it reached 120 nm at 02:00 on 21 Feb [2014](#).
970 In [the VTDMA measurements data](#), a sharp increase in the number concentration of HV particles
971 having an initial diameter of 40 nm was observed at 17:00 on 20 Feb [2014](#) (Fig. 10). This event
972 is likely related to the growth of the newly formed particles when they mixed with the volatile
973 materials [accumulated](#) via condensation or adsorption. [The volatile material which extensively](#)
974 [condensed on the pre-existing particles could be sulfate, ammonium and organics. They were](#)
975 [found to be the major species contributing to particle growth in the NPF events at different](#)
976 [locations \(Zhang et al., 2004; Smith et al., 2008; Zhang et al., 2011; Yue et al., 2016\). Zhang et](#)
977 [al. \(2004\) observed that sulfate was always the first and the fastest species to increase in](#)
978 [concentration during an NPF event. They also suggested that photochemically formed](#)
979 [secondary organics contributed significantly to the growth of the ultrafine particles. Recently,](#)
980 [Yue et al. \(2016\) reported that sulfate, ammonium and organics were the main contributors to](#)
981 [particle growth in the NPF events in Taoyuan of the PRD region.](#) As these particles aged further,
982 they grew larger as reflected in the increase in number concentrations of larger MV particles
983 and the increase in PM_{2.5} mass (Fig. 10). [Similar results were also observed in the study in](#)
984 [Beijing by Wehner et al. \(2009\). Furthermore, the](#) growth of the newly formed particles can
985 also be observed from the number size distributions of [the](#) HV, MV and LV particles at different
986 times on 20 and 21 Feb [2014](#) (Fig. 11). The mode of [the](#) HV particles increased from 40 nm at
987 17:00 to 80 nm at 21:00 on 20 Feb [2014](#). The mode stayed at 80 nm while the corresponding
988 number concentration decreased at 02:00 on 21 Feb [2014](#). In contrast, the number
989 concentrations [and diameter mode](#) of [the](#) MV particles grew continuously. The HV and MV
990 particle concentrations and diameter modes underwent much smaller changes on the non-event
991 day of 28 Feb [2014](#) (Fig. 11).

992

993 3.5 Closure analysis for LV and MV residuals at 300°C, OC and EC

994 The closure analysis of EC or the sum of EC, OC₂, OC₃, and OC₄ and the total mass of LV and
995 MV residuals ~~is was~~ conducted (Fig. 12). Good correlations ($R^2 > 0.9$) for both EC and the sum
996 of EC, OC₂, OC₃, and OC₄ with the total mass of LV and MV residuals were obtained.
997 Nonetheless, the slope for the total mass of LV and MV residuals to the mass of EC (2.94) is
998 more than two times of that for the total mass of LV and MV residuals to the sum of EC, OC₂,
999 OC₃, and OC₄ (1.22), indicating that EC alone cannot account for the total mass of LV and MV
1000 residuals. Including non-volatile OC (sum of OC₂ to OC₄) ~~give gave a~~ better mass closure with
1001 the total of LV and MV residuals. This further supports our initial postulation that the non-
1002 volatile residuals which remained intact upon heating at 300°C in the VTDMA may contain a
1003 significant amount of non-volatile OC. However, the total mass of EC, OC₂, OC₃, and OC₄ ~~do~~
1004 did not explain all the mass of LV and MV residuals. A possible explanation could be that the
1005 vaporizing temperatures of some OC₁ are close to the upper limit (310°C), hence they were not
1006 completely vaporized in the heated tube and remained in the non-volatile residuals. The
1007 presence of other refractory materials and the assumption made about the density of LV and
1008 MV are two other possible explanations.

1009 Other possible errors for the closure could be related to the different heating environments in
1010 the VTDMA and the OC/EC analyzer. In the OC/EC analyzer, OC was measured when the
1011 samples were heated in the presence of a non-oxidative carrier gas (He). In the VTDMA,
1012 aerosols were heated in air which contained O₂. Therefore, some “OC₂₋₄” that evaporated at
1013 475°C or above in the OC/EC analyzer may have been oxidized at 300°C in the VTDMA.
1014 Charring of organic matter could also occur (Philippin et al., 2004). Further study is needed to
1015 quantify the effect of oxygen on the oxidation of OC in the VTDMA. The extrapolated
1016 lognormal fitting of the size distribution of non-volatile particles can also cause errors if the
1017 mode diameter of the fitting is beyond the VTDMA’s range of measurements. While the
1018 VTDMA measured the size distribution of particles between 10 nm and 400 nm in diameter,
1019 the OC/EC analyzer took into account particles up to 2.5 μm in diameter. Yu et al. (2010)
1020 reported three EC and OC modes between ~~0.4-400 nm~~ and 10 μm in ambient aerosols in
1021 Guangzhou: ~~0.4-400 nm~~, 900 nm~~0.9~~ and 5 μm. The ~~0.4-400 nm~~ mode accounted for 44% to
1022 49% of the measured EC but only 17% to 20% of the measured OC.

1023

1024 4 Conclusions

1025 This study presents the first VTDMA measurements in a suburban area of Guangzhou in the
1026 Pearl River Delta region, China during wintertime. The LV fraction non-volatile material at
1027 300°C in VTDMA measurements was assumed to be EC particles and non-volatile OC. These
1028 partieles The LV particles, representing non-volatile material externally mixed with the volatile
1029 material, were externally mixed with volatile materials at 300°C and, contributed to less than
1030 20% of the total particle number concentration at the sampling site. The diurnal variations in
1031 the number and volume fractions of LV, MV and HV were much less obvious in this study than
1032 in other studies (e.g. Rose et al., 2011; Cheng et al., 2012; Zhang et al., 2016) likely because of
1033 the more stable atmosphere and poorer dilution of aged aerosols in winter. The back trajectory
1034 analysis-analyses showed that the measured PM_{2.5}, EC and OC concentrations were higher when
1035 the sampling site came under the influence of maritime and coastal air masses originating from
1036 the east or northeast of the site. These observations are-were attributed to the high pressure
1037 system on-the continent, the prevailing northerly wind and the enhanced pollution from north
1038 China in winter. The long-range transport continental trajectories were often associated with
1039 the cold front periods during which the dispersion of pollutants was promoted. The number
1040 fractions of LV, MV and HV particles did not show much variations among the trajectory
1041 clusters, likely because the air masses in all the clusters were transported at low altitudes (below
1042 1500 m) for over 40 h. They were therefore well-aged upon arrival at the site.

1043 While previous studies have demonstrated-indicated soot as a major component of the non-
1044 volatile residuals at 300°C measured by the VTDMA (e.g. Philippin et al., 2004; Frey et al.,
1045 2008), Häkkinen et al. (2012) and this work identified non-volatile organics as another possible
1046 component. The diurnal variations in the LV fractions and the size of the MV residuals may be
1047 related to the variation in the abundance of both EC and non-volatile OC, which evaporated at
1048 475°C and above in the OC/EC analyzer. The analyses of the diurnal variations in the LV
1049 fractions and the *VFR* of MV particles, the latter of which reflects the change in size of the non-
1050 volatile materials in the MV particles, suggest that the increase in the non-volatile fractions and
1051 in the size in the early afternoon may be related to the increase in non-volatile OC in addition
1052 to the effects of EC-coagulation and condensation. The mass closure analysis of EC and the
1053 total mass of LV and MV residuals also indicated that EC alone cannot account for the mass of
1054 the non-volatile residuals. The total mass of EC and and non-volatile OC gave a better closure
1055 with and the total mass of the LV and MV residuals, suggesting also-suggest that the non-volatile
1056 OC may have contributed to the non-volatile residuals in our VTDMA measurements.

1057 **Acknowledgements**

1058 This work is supported by the Research Grants Council of the Hong Kong Special
1059 Administrative Region, China (Project No. 600413), the Natural Science Foundation of China
1060 (Grant 41375156), Special Research and Development Fund for Research Institutes
1061 (2014EG137243) and the National Key Project of Basic Research (2011CB403403).

1062

1063

1064 **References**

- 1065 Andreae, M. O., Schmid, O., Yang, H., Chand, D., Zhen Yu, J., Zeng, L.-M., and Zhang, Y.-H.:
1066 Optical properties and chemical composition of the atmospheric aerosol in urban
1067 Guangzhou, China, *Atmos. Environ.*, 42, 6335-6350, 2008.
- 1068 Birch, M. E. and Cary, R. A.: Elemental carbon-based method for monitoring occupational
1069 exposures to particulate diesel exhaust, *Aerosol Sci. Technol.*, 25, 221-241, 1996.
- 1070 Bond, T. C.: Spectral dependence of visible light absorption by carbonaceous particles emitted
1071 from coal combustion, *Geophys. Res. Lett.*, 28, 4075-4078, 2001.
- 1072 Bradsher, K.: Trucks power China's economy, at a suffocating cost.: available at:
1073 <http://www.nytimes.com/2007/12/08/world/asia/08trucks.html>, 2007.
- 1074 Brooks, B. J., Smith, M. H., Hill, M. K., and O'Dowd, C. D.: Size-differentiated volatility
1075 analysis of internally mixed laboratory-generated aerosol, *J. Aerosol Sci*, 33, 555-579,
1076 2002.
- 1077 Chan, C. K. and Yao, X.: Air pollution in mega cities in China, *Atmos. Environ.*, 42, 1-42, 2008.
- 1078 Chen, B., Du, K., Wang, Y., Chen, J., Zhao, J., Wang, K., Zhang, F., and Xu, L.: Emission and
1079 transport of carbonaceous aerosols in urbanized coastal areas in China, *Aerosol Air Qual.*
1080 *Res.*, 12, 371-378, 2012.
- 1081 Chen, Y. and Bond, T. C.: Light absorption by organic carbon from wood combustion, *Atmos.*
1082 *Chem. Phys.*, 10, 1773-1787, 2010.
- 1083 Cheng, Y., He, K., Duan, F., Zheng, M., Du, Z., Ma, Y., and Tan, J.: Ambient organic carbon to
1084 elemental carbon ratios: Influences of the measurement methods and implications,
1085 *Atmos. Environ.*, 45, 2060-2066, 2011.
- 1086 Cheng, Y. F., Eichler, H., Wiedensohler, A., Heintzenberg, J., Zhang, Y. H., Hu, M., Herrmann,
1087 H., Zeng, L. M., Liu, S., Gnauk, T., Brüggemann, E., and He, L. Y.: Mixing state of
1088 elemental carbon and non-light-absorbing aerosol components derived from in situ
1089 particle optical properties at Xinken in Pearl River Delta of China, *J. Geophys. Res.-*
1090 *Atmos.*, 111, D20204, 2006.
- 1091 Cheng, Y. F., Su, H., Rose, D., Gunthe, S. S., Berghof, M., Wehner, B., Achtert, P., Nowak, A.,
1092 Takegawa, N., Kondo, Y., Shiraiwa, M., Gong, Y. G., Shao, M., Hu, M., Zhu, T., Zhang,
1093 Y. H., Carmichael, G. R., Wiedensohler, A., Andreae, M. O., and Pöschl, U.: Size-
1094 resolved measurement of the mixing state of soot in the megacity Beijing, China: diurnal
1095 cycle, aging and parameterization, *Atmos. Chem. Phys.*, 12, 4477-4491, 2012.
- 1096 Chow, J. C., Watson, J. G., Lowenthal, D. H., Solomon, P. A., Magliano, K. L., Ziman, S. D.,

1097 and Richards, L. W.: PM10 and PM2.5 compositions in California's San Joaquin Valley,
1098 *Aerosol Sci. Technol.*, 18, 105-128, 1993.

1099 Chow, J. C., Watson, J. G., Lu, Z., Lowenthal, D. H., Frazier, C. A., Solomon, P. A., Thuillier,
1100 R. H., and Magliano, K.: Descriptive analysis of PM2.5 and PM10 at regionally
1101 representative locations during SJVAQS/AUSPEX, *Atmos. Environ.*, 30, 2079-2112,
1102 1996.

1103 Chow, J. C., Yu, J. Z., Watson, J. G., Hang Ho, S. S., Bohannon, T. L., Hays, M. D., and Fung,
1104 K. K.: The application of thermal methods for determining chemical composition of
1105 carbonaceous aerosols: A review, *J. Environ. Sci. Heal. A*, 42, 1521-1541, 2007.

1106 Donahue, N. M., Robinson, A. L., and Pandis, S. N.: Atmospheric organic particulate matter:
1107 From smoke to secondary organic aerosol, *Atmos. Environ.*, 43, 94-106, 2009.

1108 Frey, A., Rose, D., Wehner, B., Müller, T., Cheng, Y., Wiedensohler, A., and Virkkula, A.:
1109 Application of the Volatility-TDMA Technique to Determine the Number Size
1110 Distribution and Mass Concentration of Less Volatile Particles, *Aerosol Sci. Technol.*,
1111 42, 817-828, 2008.

1112 Fuller, K. A., Malm, W. C., and Kreidenweis, S. M.: Effects of mixing on extinction by
1113 carbonaceous particles, *J. Geophys. Res.-Atmos.*, 104, 15941-15954, 1999.

1114 Ghazi, R. and Olfert, J. S.: Coating Mass Dependence of Soot Aggregate Restructuring due to
1115 Coatings of Oleic Acid and Dioctyl Sebacate, *Aerosol Sci. Technol.*, 47, 192-200, 2012.

1116 Gnauk, T., Müller, K., van Pinxteren, D., He, L.-Y., Niu, Y., Hu, M., and Herrmann, H.: Size-
1117 segregated particulate chemical composition in Xinken, Pearl River Delta, China:
1118 OC/EC and organic compounds, *Atmos. Environ.*, 42, 6296-6309, 2008.

1119 Gu, J., Du, S., Han, D., Hou, L., Yi, J., Xu, J., Liu, G., Han, B., Yang, G., and Bai, Z.-P.: Major
1120 chemical compositions, possible sources, and mass closure analysis of PM2.5 in Jinan,
1121 China, *Air Qual. Atmos. Heal.*, 7, 251-262, 2014.

1122 Häkkinen, S. A. K., Äijälä, M., Lehtipalo, K., Junninen, H., Backman, J., Virkkula, A.,
1123 Nieminen, T., Vestenius, M., Hakola, H., Ehn, M., Worsnop, D. R., Kulmala, M., Petäjä,
1124 T., and Riipinen, I.: Long-term volatility measurements of submicron atmospheric
1125 aerosol in Hyytiälä, Finland, *Atmos. Chem. Phys.*, 12, 10771-10786, 2012.

1126 Hansen, A. D. A., Rosen, H., and Novakov, T.: The Aethalometer - An Instrument for the Real-
1127 Time Measurement of Optical-Absorption by Aerosol-Particles *Sci. Total Environ.*, 36,
1128 191-196, 1984.

1129 Hitzenberger, R., Jennings, S. G., Larson, S. M., Dillner, A., Cachier, H., Galambos, Z., Rouc,

1130 A., and Spain, T. G.: Intercomparison of measurement methods for black carbon
1131 aerosols, *Atmos. Environ.*, 33, 2823-2833, 1999.

1132 Horvath, H.: Atmospheric light absorption—A review, *Atmos. Environ.*, 27, 293-317, 1993.

1133 Huffman, J. A., Docherty, K. S., Aiken, A. C., Cubison, M. J., Ulbrich, I. M., DeCarlo, P. F.,
1134 Sueper, D., Jayne, J. T., Worsnop, D. R., Ziemann, P. J., and Jimenez, J. L.: Chemically-
1135 resolved aerosol volatility measurements from two megacity field studies, *Atmos. Chem.*
1136 *Phys.*, 9, 7161-7182, 2009.

1137 Japar, S. M., Brachaczek, W. W., Gorse Jr, R. A., Norbeck, J. M., and Pierson, W. R.: The
1138 contribution of elemental carbon to the optical properties of rural atmospheric aerosols,
1139 *Atmos. Environ.*, 20, 1281-1289, 1986.

1140 Kalberer, M., Paulsen, D., Sax, M., Steinbacher, M., Dommen, J., Prevot, A. S. H., Fisseha, R.,
1141 Weingartner, E., Frankevich, V., Zenobi, R., and Baltensperger, U.: *Science*, 303, 1659,
1142 2004.

1143 Kirchstetter, T. W., Novakov, T., and Hobbs, P. V.: Evidence that the spectral dependence of
1144 light absorption by aerosols is affected by organic carbon, *J. Geophys. Res.-Atmos.*, 109,
1145 D21208, 2004.

1146 Lavanchy, V. M. H., Gäggeler, H. W., Nyeki, S., and Baltensperger, U.: Elemental carbon (EC)
1147 and black carbon (BC) measurements with a thermal method and an aethalometer at the
1148 high-alpine research station Jungfraujoch, *Atmos. Environ.*, 33, 2759-2769, 1999.

1149 Lee, B. P., Li, Y. J., Yu, J. Z., Louie, P. K. K., and Chan, C. K.: Physical and chemical
1150 characterization of ambient aerosol by HR-ToF-AMS at a suburban site in Hong Kong
1151 during springtime 2011, *J. Geophys. Res.-Atmos.*, 118, 8625-8639, 2013.

1152 Levy, M. E., Zhang, R., Zheng, J., Tan, H., Wang, Y., Molina, L. T., Takahama, S., Russell, L.
1153 M., and Li, G.: Measurements of submicron aerosols at the California–Mexico border
1154 during the Cal–Mex 2010 field campaign, *Atmos. Environ.*, 88, 308-319, 2014.

1155 Liousse, C., Cachier, H., and Jennings, S. G.: Optical and thermal measurements of black
1156 carbon aerosol content in different environments: Variation of the specific attenuation
1157 cross-section, σ , *Atmos. Environ.*, 27, 1203-1211, 1993.

1158 Lo, J. C. F., Lau, A. K. H., Fung, J. C. H., and Chen, F.: Investigation of enhanced cross-city
1159 transport and trapping of air pollutants by coastal and urban land-sea breeze circulations,
1160 *J. Geophys. Res.-Atmos.*, 111, D14104, 2006.

1161 Murphy, B. N., Donahue, N. M., Robinson, A. L., and Pandis, S. N.: A naming convention for
1162 atmospheric organic aerosol, *Atmos. Chem. Phys.*, 14, 5825-5839, 2014.

1163 Novakov, T., Ramanathan, V., Hansen, J. E., Kirchstetter, T. W., Sato, M., Sinton, J. E., and
1164 Sathaye, J. A.: Large historical changes of fossil-fuel black carbon aerosols, *Geophys.*
1165 *Res. Lett.*, 30, 4, 2003.

1166 Onasch, T. B., Trimborn, A., Fortner, E. C., Jayne, J. T., Kok, G. L., Williams, L. R., Davidovits,
1167 P., and Worsnop, D. R.: Soot Particle Aerosol Mass Spectrometer: Development,
1168 Validation, and Initial Application, *Aerosol Sci. Technol.*, 46, 804-817, 2012.

1169 Penner, J. E. and Novakov, T.: Carbonaceous particles in the atmosphere: A historical
1170 perspective to the Fifth International Conference on Carbonaceous Particles in the
1171 Atmosphere, *J. Geophys. Res.-Atmos.*, 101, 19373-19378, 1996.

1172 Petzold, A. and Schönlinner, M.: Multi-angle absorption photometry—a new method for the
1173 measurement of aerosol light absorption and atmospheric black carbon, *J. Aerosol Sci.*,
1174 35, 421-441, 2004.

1175 Philippin, S., Wiedensohler, A., and Stratmann, F.: Measurements of non-volatile fractions of
1176 pollution aerosols with an eight-tube volatility tandem differential mobility analyzer
1177 (VTDMA-8), *J. Aerosol Sci.*, 35, 185-203, 2004.

1178 Pinnick, R., Jennings, S., and Fernandez, G.: Volatility of aerosols in the arid southwestern
1179 United States, *J. Atmos. Sci.*, 44, 562-576, 1987.

1180 Putaud, J. P., Van Dingenen, R., Alastuey, A., Bauer, H., Birmili, W., Cyrys, J., Flentje, H.,
1181 Fuzzi, S., Gehrig, R., Hansson, H. C., Harrison, R. M., Herrmann, H., Hitzenberger, R.,
1182 Hüglin, C., Jones, A. M., Kasper-Giebl, A., Kiss, G., Koussa, A., Kuhlbusch, T. A. J.,
1183 Löschau, G., Maenhaut, W., Molnar, A., Moreno, T., Pekkanen, J., Perrino, C., Pitz, M.,
1184 Puxbaum, H., Querol, X., Rodriguez, S., Salma, I., Schwarz, J., Smolik, J., Schneider,
1185 J., Spindler, G., ten Brink, H., Tursic, J., Viana, M., Wiedensohler, A., and Raes, F.: A
1186 European aerosol phenomenology – 3: Physical and chemical characteristics of
1187 particulate matter from 60 rural, urban, and kerbside sites across Europe, *Atmos.*
1188 *Environ.*, 44, 1308-1320, 2010.

1189 Rader, D. J. and McMurry, P. H.: Application of the tandem differential mobility analyzer to
1190 studies of droplet growth or evaporation, *J. Aerosol Sci.*, 17, 771-787, 1986.

1191 Robinson, A. L., Donahue, N. M., Shrivastava, M. K., Weitkamp, E. A., Sage, A. M., Grieshop,
1192 A. P., Lane, T. E., Pierce, J. R., and Pandis, S. N.: Rethinking organic aerosols:
1193 Semivolatile emissions and photochemical aging, *Science*, 315, 1259-1262, 2007.

1194 Rolph, G. D.: Real-time Environmental Applications and Display sYstem (READY) Website
1195 (<http://www.ready.noaa.gov>). NOAA Air Resources Laboratory, College Park, MD.,

1196 2016.

1197 Rose, D., Wehner, B., Ketzler, M., Engler, C., Voigtländer, J., Tuch, T., and Wiedensohler, A.:

1198 Atmospheric number size distributions of soot particles and estimation of emission

1199 factors, *Atmos. Chem. Phys.*, 6, 1021-1031, 2006.

1200 Rose, D., Gunthe, S. S., Su, H., Garland, R. M., Yang, H., Berghof, M., Cheng, Y. F., Wehner,

1201 B., Achtert, P., Nowak, A., Wiedensohler, A., Takegawa, N., Kondo, Y., Hu, M., Zhang,

1202 Y., Andreae, M. O., and Pöschl, U.: Cloud condensation nuclei in polluted air and

1203 biomass burning smoke near the mega-city Guangzhou, China – Part 2: Size-resolved

1204 aerosol chemical composition, diurnal cycles, and externally mixed weakly CCN-active

1205 soot particles, *Atmos. Chem. Phys.*, 11, 2817-2836, 2011.

1206 Rosen, H., Hansen, A. D. A., Gundel, L., and Novakov, T.: Identification of the optically

1207 absorbing component in urban aerosols, *Appl. Opt.*, 17, 3859-3861, 1978.

1208 Schauer, J. J., Mader, B. T., Deminter, J. T., Heidemann, G., Bae, M. S., Seinfeld, J. H., Flagan,

1209 R. C., Cary, R. A., Smith, D., Huebert, B. J., Bertram, T., Howell, S., Kline, J. T., Quinn,

1210 P., Bates, T., Turpin, B., Lim, H. J., Yu, J. Z., Yang, H., and Keywood, M. D.: ACE-Asia

1211 intercomparison of a thermal-optical method for the determination of particle-phase

1212 organic and elemental carbon, *Environ. Sci. Technol.*, 37, 993-1001, 2003.

1213 Smith, J. N., Dunn, M. J., VanReken, T. M., Iida, K., Stolzenburg, M. R., McMurry, P. H., and

1214 Huey, L. G.: Chemical composition of atmospheric nanoparticles formed from

1215 nucleation in Tecamac, Mexico: Evidence for an important role for organic species in

1216 nanoparticle growth, *Geophys. Res. Lett.*, 35, L04808, 2008.

1217 Stein, A. F., Draxler, R. R., Rolph, G. D., Stunder, B. J. B., Cohen, M. D., and Ngan, F.: NOAA's

1218 HYSPLIT Atmospheric Transport and Dispersion Modeling System, *B. Am. Meteorol.*

1219 *Soc.*, 96, 2059-2077, 2015.

1220 Stephens, M., Turner, N., and Sandberg, J.: Particle identification by laser-induced

1221 incandescence in a solid-state laser cavity, *Appl. Opt.*, 42, 3726-3736, 2003.

1222 Tan, H. B., Yin, Y., Gu, X. S., Li, F., Chan, P. W., Xu, H. B., Deng, X. J., and Wan, Q. L.: An

1223 observational study of the hygroscopic properties of aerosols over the Pearl River Delta

1224 region, *Atmos. Environ.*, 77, 817-826, 2013a.

1225 Tan, H. B., Xu, H. B., Wan, Q. L., Li, F., Deng, X. J., Chan, P. W., Xia, D., and Yin, Y.: Design

1226 and Application of an Unattended Multifunctional H-TDMA System, *J. Atmos. Ocean*

1227 *Tech.*, 30, 1136-1148, 2013b.

1228 Tao, J., Zhang, L., Ho, K., Zhang, R., Lin, Z., Zhang, Z., Lin, M., Cao, J., Liu, S., and Wang,

1229 G.: Impact of PM_{2.5} chemical compositions on aerosol light scattering in Guangzhou
1230 — the largest megacity in South China, *Atmos. Res.*, 135–136, 48-58, 2014.

1231 Turpin, B. J., Cary, R. A., and Huntzicker, J. J.: An In Situ, Time-Resolved Analyzer for Aerosol
1232 Organic and Elemental Carbon, *Aerosol Sci. Technol.*, 12, 161-171, 1990.

1233 Twomey, S.: On the composition of cloud nuclei in the northeastern United States, *J. Rech.*
1234 *Atmos.*, 3, 281-285, 1968.

1235 Villani, P., Picard, D., Marchand*, N., and Laj, P.: Design and Validation of a 6-Volatility
1236 Tandem Differential Mobility Analyzer (VTDMA), *Aerosol Sci. Technol.*, 41, 898-906,
1237 2007.

1238 Virkkula, A., Ahlquist, N. C., Covert, D. S., Arnott, W. P., Sheridan, P. J., Quinn, P. K., and
1239 Coffman, D. J.: Modification, Calibration and a Field Test of an Instrument for
1240 Measuring Light Absorption by Particles, *Aerosol Sci. Technol.*, 39, 68-83, 2005.

1241 Wehner, B., Philippin, S., Wiedensohler, A., Scheer, V., and Vogt, R.: Variability of non-volatile
1242 fractions of atmospheric aerosol particles with traffic influence, *Atmos. Environ.*, 38,
1243 6081-6090, 2004.

1244 Wehner, B., Berghof, M., Cheng, Y. F., Achtert, P., Birmili, W., Nowak, A., Wiedensohler, A.,
1245 Garland, R. M., Pöschl, U., Hu, M., and Zhu, T.: Mixing state of nonvolatile aerosol
1246 particle fractions and comparison with light absorption in the polluted Beijing region, *J.*
1247 *Geophys. Res.-Atmos.*, 114, D00G17, 2009.

1248 Wu, C., Ng, W. M., Huang, J. X., Wu, D., and Yu, J. Z.: Determination of Elemental and Organic
1249 Carbon in PM_{2.5} in the Pearl River Delta Region: Inter-Instrument (Sunset vs. DRI
1250 Model 2001 Thermal/Optical Carbon Analyzer) and Inter-Protocol Comparisons
1251 (IMPROVE vs. ACE-Asia Protocol), *Aerosol Sci. Technol.*, 46, 610-621, 2012.

1252 Wu, D., Bi, X. Y., Deng, X. J., Li, F., Tan, H. B., Liao, G. L., and Huang, J.: Effect of
1253 atmospheric haze on the deterioration of visibility over the Pearl River Delta, *Acta*
1254 *Meteorol. Sin.*, 21, 215-223, 2007.

1255 Yu, H., Wu, C., Wu, D., and Yu, J. Z.: Size distributions of elemental carbon and its contribution
1256 to light extinction in urban and rural locations in the pearl river delta region, China,
1257 *Atmos. Chem. Phys.*, 10, 5107-5119, 2010.

1258 Yue, D. L., Zhong, L. J., Zhang, T., J., S., L., Y., Q., Y. S., Y., Z., and Zeng, L. M.: Particle
1259 Growth and Variation of Cloud Condensation Nucleus Activity on Polluted Days with
1260 New Particle Formation: A Case Study for Regional Air Pollution in the PRD Region,
1261 China, *Aerosol Air Qual. Res.*, 16, 323-335, 2016.

1262 Zhang, Q., Stanier, C. O., Canagaratna, M. R., Jayne, J. T., Worsnop, D. R., Pandis, S. N., and
1263 Jimenez, J. L.: Insights into the Chemistry of New Particle Formation and Growth
1264 Events in Pittsburgh Based on Aerosol Mass Spectrometry, *Environ. Sci. Technol.*, 38,
1265 4797-4809, 2004.

1266 Zhang, S. L., Ma, N., Kecorius, S., Wang, P. C., Hu, M., Wang, Z. B., Größ, J., Wu, Z. J., and
1267 Wiedensohler, A.: Mixing state of atmospheric particles over the North China Plain,
1268 *Atmos. Environ.*, 125, Part A, 152-164, 2016.

1269 Zhang, Y., Wang, X., Li, G., Yang, W., Huang, Z., Zhang, Z., Huang, X., Deng, W., Liu, T.,
1270 Huang, Z., and Zhang, Z.: Emission factors of fine particles, carbonaceous aerosols and
1271 traces gases from road vehicles: Recent tests in an urban tunnel in the Pearl River Delta,
1272 China, *Atmos. Environ.*, 122, 876-884, 2015.

1273 Zhang, Y. M., Zhang, X. Y., Sun, J. Y., Lin, W. L., Gong, S. L., Shen, X. J., and Yang, S.:
1274 Characterization of new particle and secondary aerosol formation during summertime
1275 in Beijing, China, *Tellus B*, 63, 382-394, 2011.

1276
1277

1278 Table 1. Temperature (T) and residence time (RT) protocol of the semi-continuous Sunset
1279 OC/EC analyzer (Wu et al., 2012)

Carbon Fraction	Carrier Gas	T (°C)	RT (s)
OC ₁	He	310	80
OC ₂		475	60
OC ₃		615	60
OC ₄		870	90
EC ₁	He and 2% O ₂	550	45
EC ₂		625	45
EC ₃		700	45
EC ₄		775	45
EC ₅		850	45
EC ₆		870	45

1280

1281

1 Table 2. Summary of average number and volume fractions in VTDMA measurements at 300°C.

Diameter (nm)	40	80	110	150	200	300
Number fraction						
CV	0.380 ± 0.153	0.174 ± 0.097	0.188 ± 0.081	0.167 ± 0.074	0.153 ± 0.070	0.141 ± 0.065
HV	0.255 ± 0.097	0.198 ± 0.052	0.165 ± 0.055	0.163 ± 0.064	0.178 ± 0.081	0.214 ± 0.097
MV	0.314 ± 0.097	0.513 ± 0.089	0.515 ± 0.098	0.530 ± 0.105	0.523 ± 0.116	0.497 ± 0.125
LV	0.051 ± 0.026	0.113 ± 0.040	0.132 ± 0.041	0.140 ± 0.041	0.146 ± 0.044	0.148 ± 0.047
Volume fraction						
VM	0.503 ± 0.131	0.600 ± 0.082	0.580 ± 0.073	0.590 ± 0.066	0.602 ± 0.064	0.627 ± 0.064
CV	0.361 ± 0.168	0.163 ± 0.105	0.166 ± 0.098	0.148 ± 0.086	0.134 ± 0.080	0.127 ± 0.073
HV	0.014 ± 0.005	0.011 ± 0.003	0.008 ± 0.002	0.007 ± 0.003	0.007 ± 0.003	0.007 ± 0.003
MV	0.070 ± 0.025	0.112 ± 0.024	0.112 ± 0.025	0.115 ± 0.026	0.109 ± 0.027	0.091 ± 0.025
LV	0.052 ± 0.026	0.114 ± 0.040	0.134 ± 0.044	0.140 ± 0.042	0.148 ± 0.048	0.148 ± 0.047

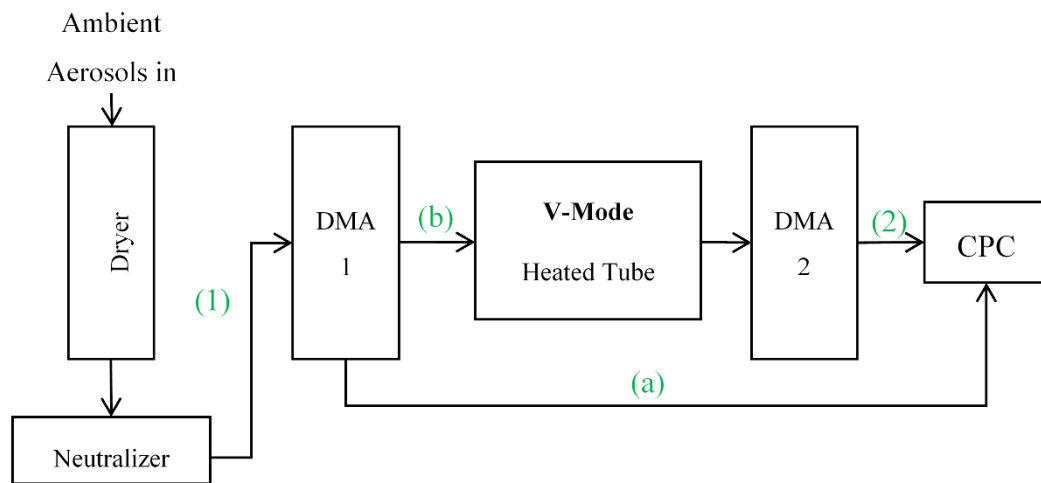
2

1 Table 3. Summary of concentrations of PM_{2.5}, OC, EC and the ratio of OC to EC (OC/EC) in
 2 the five clusters.

	Cluster				
	Coastal	Maritime		Continental	
	1	2	3	4	5
Origin (to the site)	NE	NE/E	NE	NW	NW
PM _{2.5} (µg m ⁻³)	58.5 ± 24.4	58.9 ± 30.9	47.5 ± 28.4	33.9 ± 15.9	33.8 ± 19.3
OC (µg m ⁻³)	10.8 ± 6.01	10.84 ± 7.22	10.13 ± 6.89	5.51 ± 3.3	7.32 ± 2.75
EC (µg m ⁻³)	4.38 ± 2.97	4.98 ± 4.21	3.43 ± 3.12	1.8 ± 0.98	2.46 ± 0.59
OC/EC	2.83 ± 1.05	2.62 ± 1.03	3.65 ± 1.6	3.18 ± 1.26	2.94 ± 0.73

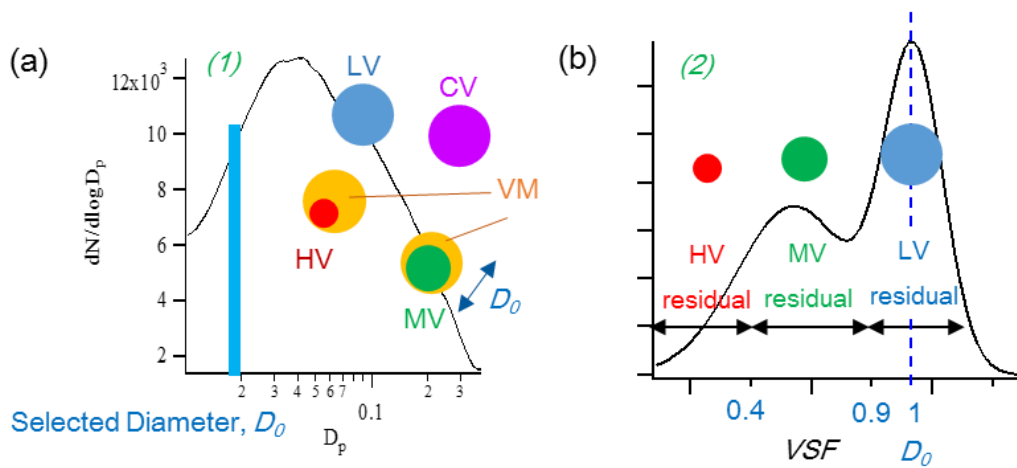
3

4

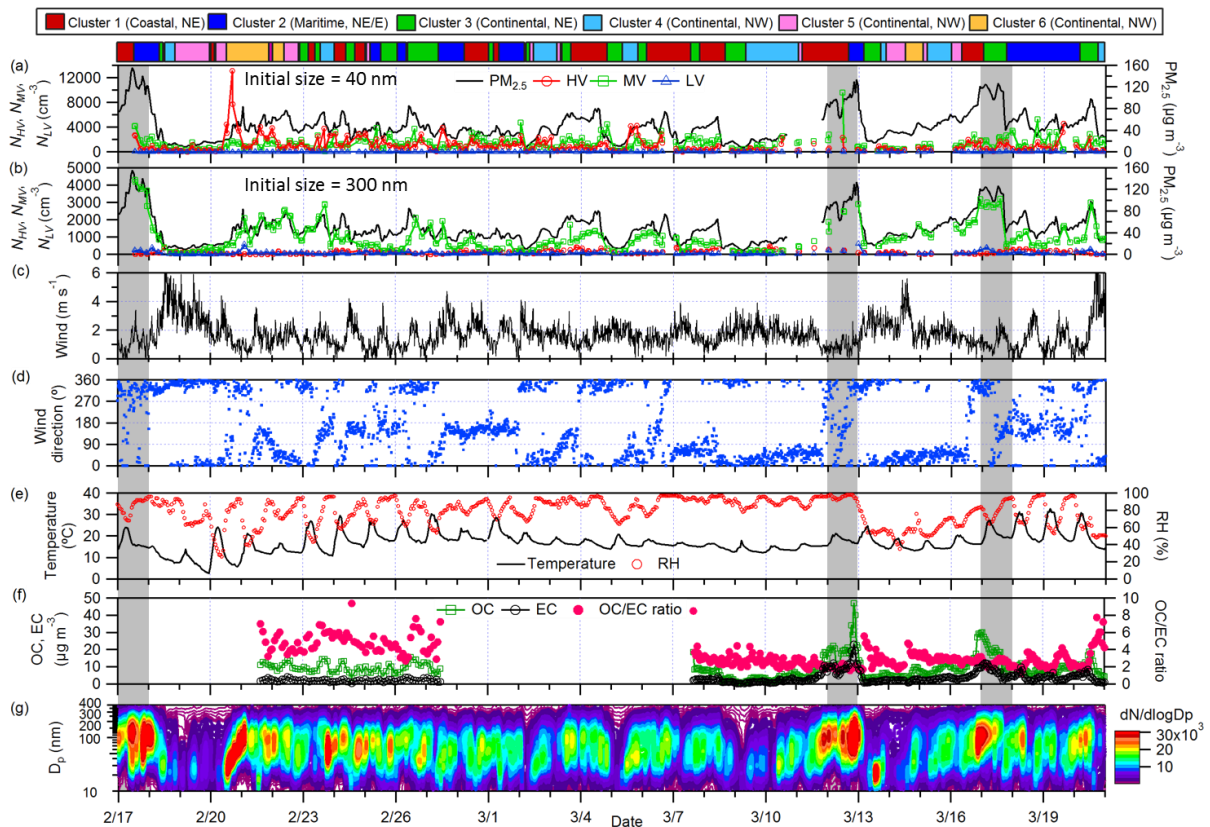


1
2
3

Fig. 1. A Schematic diagram of the volatility tandem differential mobility analyzer (VTDMA).

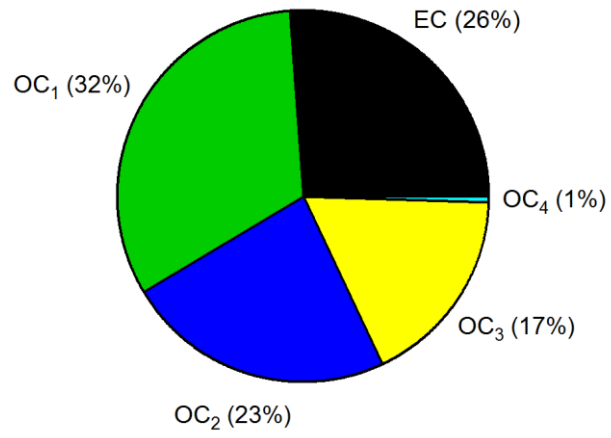


1
 2 Fig. 2. Examples of particle size distributions of (a) ambient aerosols before entering DMA₁
 3 and (b) residuals of the size-selected particles (D_0) after heating. at 300°C. The distributions in
 4 Fig. 2a and 2b correspond to (1) and (2) in Figure 1 respectively. Residuals are divided into
 5 three groups—LV (blue), MV (green) and HV (red)—based on their *VSF*. CV (purple) and VM
 6 (orange) are vaporized and hence not measured as residuals. VM appears as coating for
 7 illustration purposes only. It does not necessarily reflect the morphology of the particles.
 8



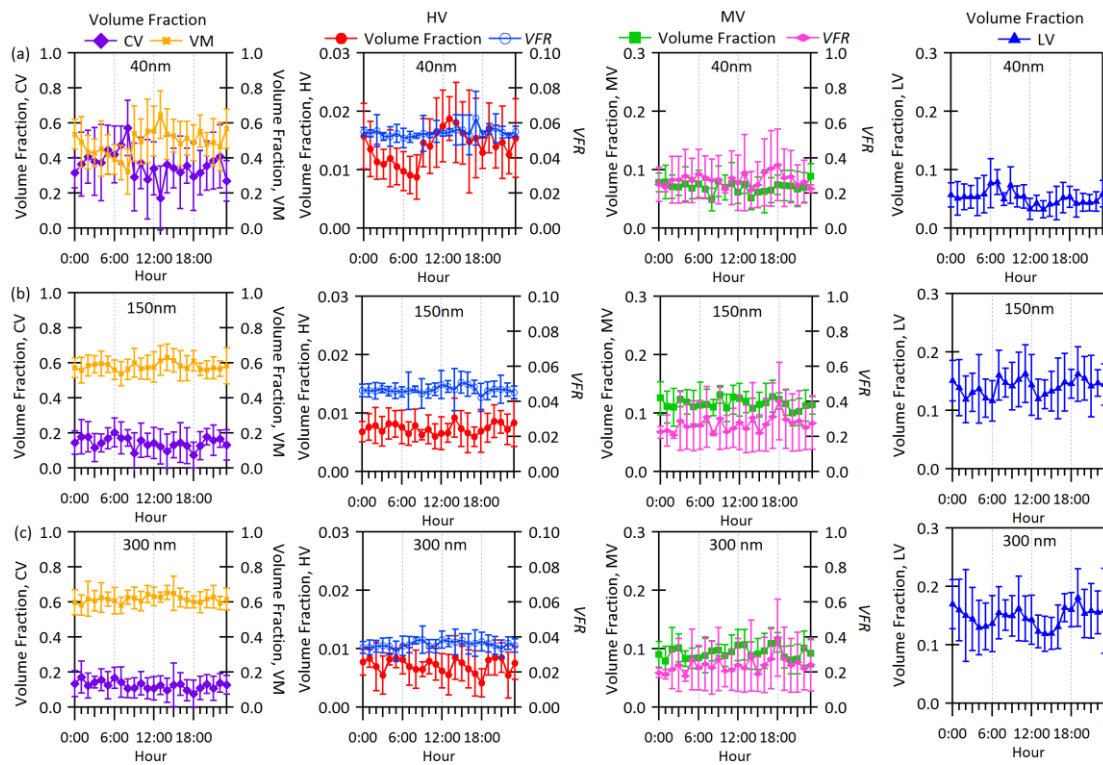
1
 2 Fig. 3. Temporal variation of number concentrations of HV, MV and LV in 40 nm and 300 nm
 3 particles, $PM_{2.5}$, major meteorological parameters, OC and EC concentrations, OC-to-EC ratio
 4 and particle number size distributions in the campaign. Air mass clusters are depicted at the top
 5 and the shaded areas indicate days with daily-averaged $PM_{2.5}$ concentrations exceeding $95 \mu g$
 6 m^{-3} .

7
 8
 9



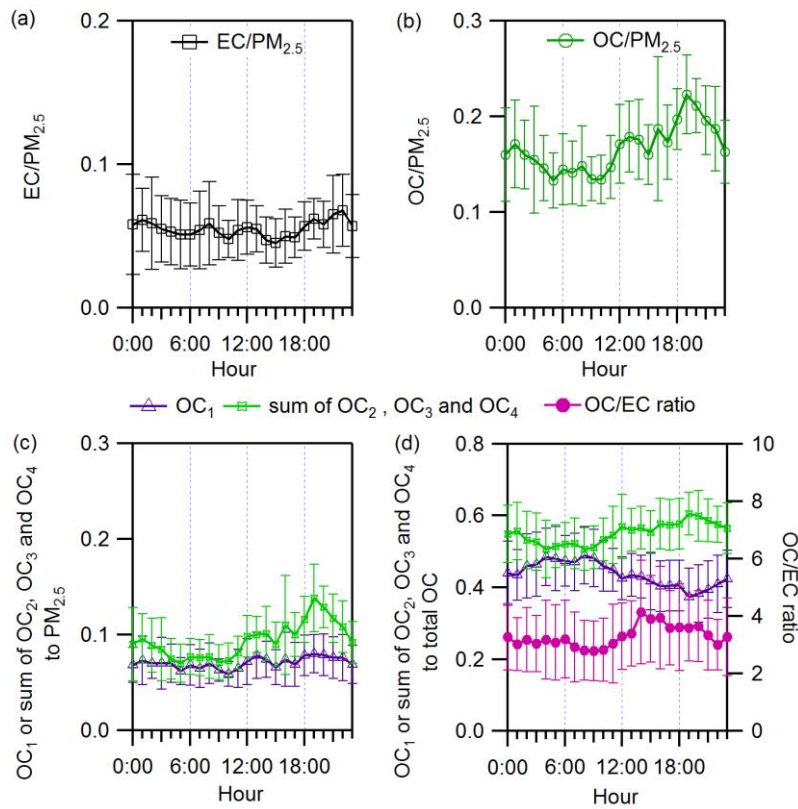
1
2
3
4
5

Fig. 4. Average mass fractions of EC, OC₁, OC₂, OC₃ and OC₄ in PM_{2.5}.



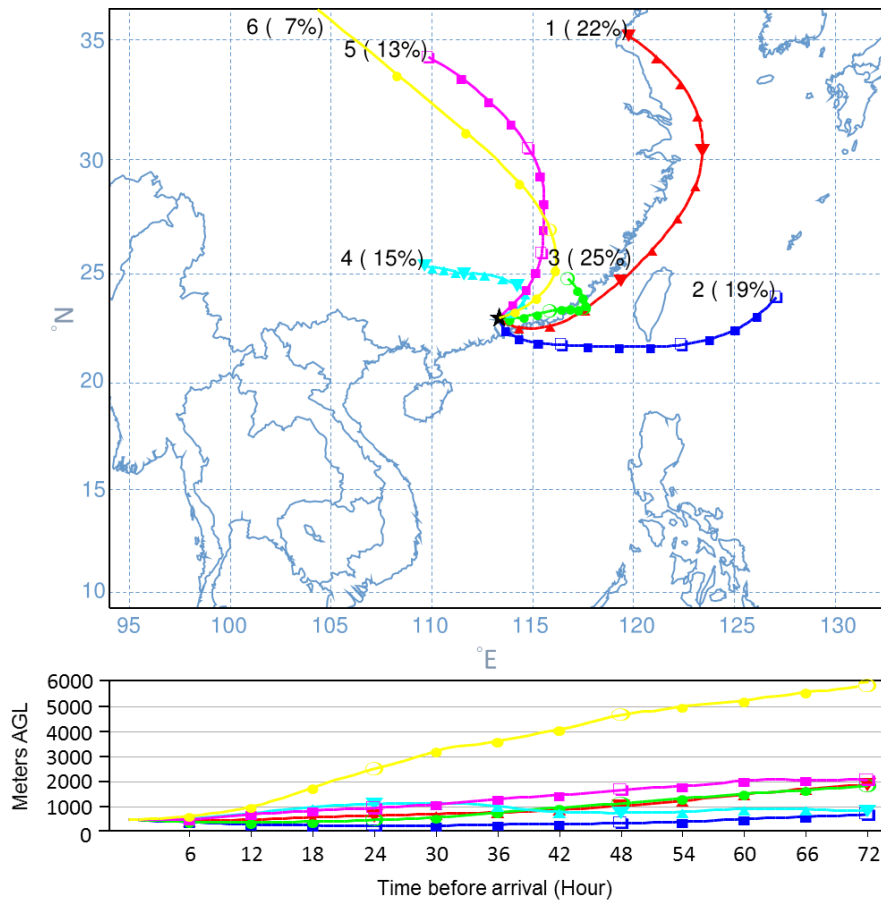
1
 2 Fig. 5. Diurnal variations in the volume fractions of (columns from left to right) CV, VM, HV
 3 residuals, MV residuals and LV residuals in (a) 40 nm, (b) 150 nm and (c) 300 nm particles in
 4 February and March 2014. Diurnal variations in the volume fraction remaining (*VFR*) of HV
 5 and MV particles are plotted on the right axis. Error bars represent one standard deviation.

6
 7



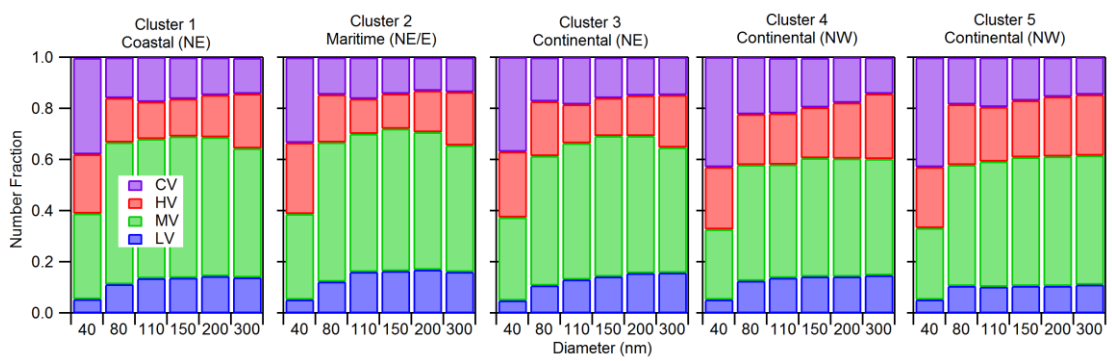
1
2
3
4
5
6

Fig. 6. Diurnal variations in the mass fractions of EC, OC, OC₁ and the sum of OC₂, OC₃ and OC₄ in PM_{2.5}, the ratio of OC to EC, mass fractions of OC₁ and the sum of OC₂, OC₃ and OC₄ to total OC in February and March 2014. Error bars represent one standard deviation.



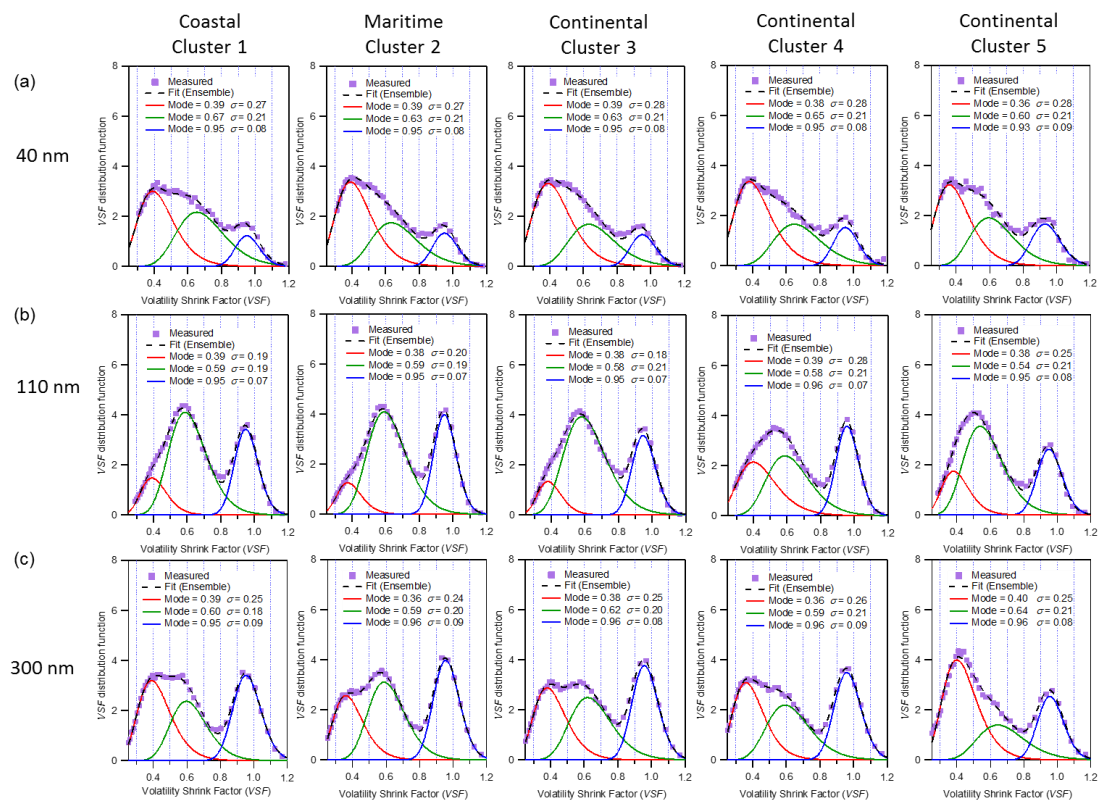
1
2
3
4
5

Fig. 7. Mean back trajectories of the six types of air masses arriving at the sampling site.



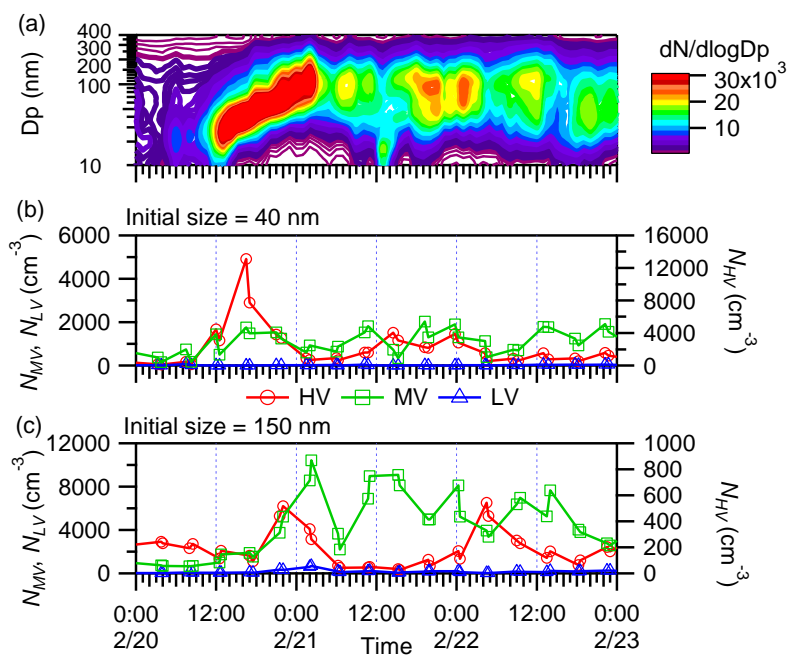
1
 2 Fig. 8. Average number fractions of CV, HV, MV and LV in clusters 1 to 5 at different selected
 3 diameters.

4



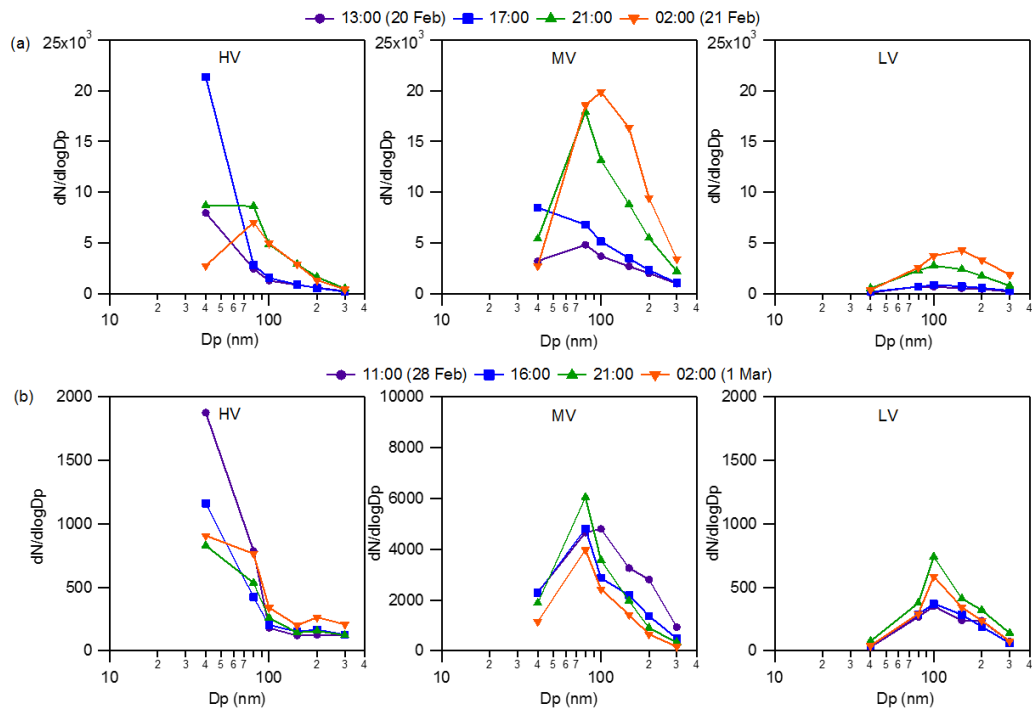
1
 2 Fig. 9. Volatility shrink factor (*VSF*) distribution function in different clusters. Solid and dotted
 3 lines are the peaks fitted with log-normal function and the ensemble distributions, respectively.

4



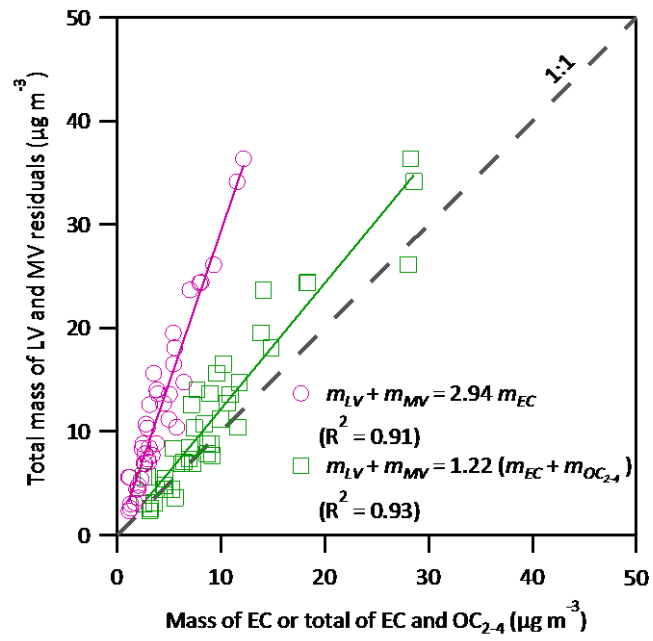
1
 2 Fig. 10. Time series of (a) particle number size distribution, (b) number concentrations of HV,
 3 MV and LV in 40 nm particles and (c) number concentrations of HV, MV and LV in 150 nm
 4 particles during a new particle event day on 20 Feb 2014.

5



1
 2 Fig. 11. Particle number size distribution of (columns from left to right) HV, MV and LV
 3 particles (a) during a new particle formation event at 13:00, 17:00, 21:00 on 20 Feb and 02:00
 4 on 21 Feb 2014 and (b) during non-event days at 11:00, 16:00, 21:00 on 28 Feb and 02:00 on 1
 5 Mar 2014.

6
 7
 8



1
2
3
4
5

Fig. 12. Aclosure analysis of the total mass of LV and MV residuals from VTDMA at 300°C and measured mass of EC or total of EC and OC₂₋₄ from the OC/EC analyzer.